ENSO Teleconnections to the Indian Summer Monsoon in Observations and Models

Indrani Roy, Renata G. Tedeschi and Matthew Collins

College of Engineering, Mathematics and Physical Sciences
University of Exeter
Laver Building
Streatham Campus
North Park Road
Exeter
UK
EX4 4QE

Abstract.

The teleconnections of different types of El Niño Southern Oscillation (ENSO) to the Indian Summer Monsoon are investigated in observations and models. We find that, not all regions in India are strongly affected by ENSO, so we focus on two regional teleconnections i) a negative rainfall signal around Central North East (CNE) India and 'Hilly' region during El Niño (and vice versa for La Niña) and, ii) similar signal for parts of Southern Peninsular region. Using correlations, it is found that more than 50% of the CMIP5 models capture these two regional teleconnections, with first captured by more than 80% of models. Furthermore, using a compositing technique that may better capture asymmetries in the response to warm and cold events, we find that most models again agree on the sign of regional teleconnection around the CNE and Hilly region, suggesting the robustness of ENSO signal in that region. The Peninsular teleconnection is less well simulated in models. We find a clear connection between the Walker Circulation and Indian Summer Monsoon rainfall around central India in models.

Keywords: Canonical ENSO, ENSO Modoki, Indian Summer Monsoon.

1. Introduction

The Indian summer monsoon (ISM) provides up to 80% of the annual mean precipitation of the country and has enormous impacts on the Indian economy, principally through its effect on agriculture and associated industries. Being one of the most populated countries in the world, it also has a major impact on the global economy (Population Reference Bureau, 2014). The ISM is also an important part of the global-scale atmospheric circulation, as it dominates the boreal summer tropical meridional overturning and the local Hadley circulation (Trenberth et al. 2006)).

The ISM represents a large-scale heat source situated off the equator, at a mean position of around 20N but varying in the east and western parts of the subcontinent. Linear theory of the atmospheric response to such a heat source (Gill 1980) predicts a strong local Hadley circulation associated with that heat source. The ISM may be viewed as a superposition and interaction between a regional Hadley circulation and a planetary-scale Walker circulation (Goswami 1994). This view is similar to the lateral and transverse monsoons discussed in Webster et al. (1998). The regional Hadley circulation is due to the direct response of the off-equatorial monsoon heat source, while the Walker circulation is due to equatorial heat sources. The regional Hadley circulation can be affected by changes in the location and strength of the monsoon heat source. Whereas, the Walker circulation over the equatorial Indian Ocean, may be influenced remotely by the movement of equatorial heat sources in the Pacific, such as those associated with El Niño Southern Oscillation (ENSO). Studies have shown that the ISM is strongly modulated by the ENSO (e.g. Turner *et al.,* 2005; Maity and Kumar, 2006).

Sea Surface Temperature (SST) anomalies associated with El Niño and La Niña are associated with anomalous atmospheric convection and anomalous upper-level divergence, perturbing the global circulation. Rossby waves are triggered and the Hadley and Walker circulations are disturbed (e.g. Larkin and Harrison, 2005), leading to teleconnections. Different types of ENSO, defined in terms of the spatial pattern of Tropical Pacific SST, have been proposed in the literature. The Classical/Canonical or East Pacific (EP) mode is dominated by variability centred in the east Pacific. Central-Pacific (CP)/Warm Pool/Modoki modes have their SST anomalies confined to the central Pacific, (Trenberth *et al*., 2002; Larkin and Harrison, 2005; Ashok *et al*., 2007; Hill *et al*., 2009; Kug et al. 2009).

There are differences in global and local influences between ENSO Modoki and Canonical ENSO (Global: Ashok *et al*., 2007; Weng *et al*., 2007; Pacific Rim: Weng *et al*., 2009; South China Sea: Chang *et al*., 2008; Australia: Brown *et al*., 2009; Cai and Cowan, 2009; Taschetto and England, 2009; South America: Tedeschi et al. 2013; Tedeschi and Collins, 2015). For example, Ashok *et al*. (2007) showed that the impacts of Canonical and Modoki show opposing rainfall signals during June–July–August–September (JJAS) in almost whole of South America (from the equator to 40 °S). During JJAS of Canonical El Niño years, equatorial South America has rainfall deficit. During Modoki El Niño years, North Western South America receives excessive precipitation. Cai and Cowan (2009) studied La Niña Modoki impacts on precipitation over Australia in the austral autumn (March–April–May, MAM). Precipitation increases, extending from North Western Australia to the northern Murray-Darling Basin, are observed when there is a cold SST anomaly over the Dateline during La Niña Modoki. During a Canonical La Niña, the precipitation increase is shifted eastward.

In recent decades, the nature of ISM precipitation variability may have changed (Ashrit et al, 2001; IPCC, 2013), as may the frequency of occurrence of different ENSO events. Monsoon precipitation and ENSO show a weaker correlation in recent decades, with the Indian monsoon occurring with normal levels of rainfall despite the occurrence of El Niños (Kumar et a., 1999; Ashok et al., 2001; Ashrit et al, 2001). Ashok et al. (2001) showed, using data covering 1958-1997, that the Indian Ocean Dipole (IOD) and ENSO have complementarily affected the ISM during that period. They showed that when the correlation between ENSO and ISM is low, the correlation between IOD and ISM is high, and vice versa. On the other hand, ENSO Modoki events have been observed more often since 1980 (Ashok and Yamagata, 2009; Yeh et al. 2009). Roy and Collins (2014) showed that variations in the local Hadley circulation may have played a role in modulating the usual ISM ENSO teleconnection during the recent period. One hypothesis is that the increase of ENSO Modoki has extratropical connections that have the potential to influence the local Hadley circulation, which then subsequently modifies the ENSO-ISM relationship. An alternative hypothesis is put forward by Chang et al. (2001), who suggested that the weakening of Indian monsoon rainfall–ENSO relationship since 1970s is most likely due to a strengthened North Atlantic Oscillation (NAO) on interdecadal time scales. It is of interest that the ISM–ENSO relationship that weakened since the 1970s seems to have recovered toward the end of the twentieth century (Yim et al. 2013). It indicates the need to study various influences of different types of ENSO separately on the ISM.

A latest collaborative effort among various groups of modelling communities around the world has coordinated experiments comprising the 5th phase of the Coupled Model Inter-comparison Project (CMIP5) (Taylor et al., 2012). The coupled CMIP5 models are capable of simulating

ENSO-like variability in the tropical Pacific, including interannual variability in the Central and Eastern equatorial Pacific (Bellenger et al. 2014). More CMIP5 models show a realistic range of ENSO frequencies in the 2–7 year band in the eastern equatorial Pacific, than for the CMIP3 group of models. SST anomalies that peak during November to January, as seen in observations, is present in approximately half of the CMIP5 models. Comparing CMIP3 and CMIP5 models, Jourdain et al. (2013) discussed ISM precipitation in detail including its connection with ENSO. They showed that the performance of CMIP5 is improved on CMIP3. Recent study of Roy and Tedeschi (2016) also discussed ENSO ISM teleconnection, using CMIP5 models, considering various subcategory of ENSO.

Here we examine different types of ENSO in observations and models and their teleconnections with the ISM. Section 2 covers the methodology and data. Results are discussed in section 3 and conclusion drawn in section 4.

2. Methodology and Data

Different types of ENSO are defined using SST anomalies (SSTAs) in four different regions of the tropical Pacific (Fig. 1, top): Canonical region (90°W-140°W, 5°N-5°S), region A (165°E-140°W, 10°S-10°N), region B (110°W-70°W, 15°S-5°N) and region C (125°E-145°E, 10°S-20°N).

An ENSO index proposed by Ashok et al. (2007), known as the ENSO Modoki Index (EMI), can be defined as

EMI = (region A SSTA) – 0.5(region B SSTA - 0.5(region C SSTA).

We use the following definitions (Tedeschi et al, 2013; Tedeschi and Collins, 2015; Kao and Yu, 2009, Ashok et al., 2007, Kug et al, 2009):

- El Niño Modoki (ENM) if the EMI is greater than $0.7\sigma_M$, where σ_M is the standard deviation of the EMI and region A SSTAs greater than $0.7\sigma_A$, where σ_A is the standard deviation of the region A SSTAs.
- La Niña Modoki (LMN) if the EMI is less than $-0.7\sigma_M$ and region A SSTAs less than $-0.7\sigma_A$.
- ENSO Canonical (ENC/LNC) if the SSTA in the Canonical region is greater than $0.7\sigma_C$/less than $-0.7\sigma_C$, where σ_C is the standard deviation of SSTAs in that region
- ENSO Canonical and Modoki (ENCM/LNCM): if the SSTAs satisfy both the Canonical and Modoki criteria

Correlation and compositing techniques are used to quantify teleconnections and to understand the asymmetry in teleconnections for different types of ENSO events. For the compositing analysis, the additional region A feature in the definition of Modoki events is used. For the correlation analysis, the original EMI index is employed. The significance of the correlation studies are tested using student's t-test, and for compositing using the hypergeometric test (Meyer, 1970). The hypergeometric test is also used by Ropelewski and Halpert (1987), Grimm (2003, 2004) and Tedeschi et al (2013).

Bollasina et al. (2011) identified a specific region in the Central North East (CNE) India, covering a box region (76° to 87°E, 20° to 28°N) that showed a significant decreasing precipitation trend during the second half of the last century. Goswami et al. (2006) also noticed such a trend, even when extending that box region to the east of the Peninsular (74.5°E to 86.5°E and 16.5°N to 26.5°N). Those two regions are used later to define which we call CNE and PEN, and marked as CI and CII in Fig. 1 (bottom). In this study we show that the CNE and Peninsular region also suggest some distinctive features in terms of ISM ENSO teleconnection.

We analyse CMIP5 simulations from atmospheric global circulation models (AGCMs) with prescribed SST (Hurrel et al., 2008) i.e. Atmospheric Model Intercomparison Project simulations (AMIP5 1979-2008) and coupled atmosphere-ocean historical simulations for the period 1861-2005. Models those have both the versions of CMIP5 and AMIP5 are considered (altogether 23 models) and are shown in Table 1. One ensemble member from each of 23 models is included.

Models are also separated as high top or low top, as shown by H or L in Table 1, as previous studies have considered this separation when looking at extratropical ENSO teleconnections (Hurwitz et al, 2014, Charlton-Perez et al, 2013). High top models are those that have upper lids up to the Stratopause (1 hPa) and/or few model layers in the Stratosphere. Eight models fall in this category.

For ISM precipitation, observational data from Global Precipitation Climatology Project (GPCP) is used (Adler et al, 2003, Huffman et al. 2009). Data from over 6,000 rain gauge stations, and satellite geostationary and low-orbit infrared, passive microwave, and sounding observations have been merged to estimate monthly rainfall on a 2.5-degree global grid from 1979 to the present. The combination of satellite-based rainfall estimates provides the most complete analysis of rainfall available to date over the global oceans, and adds necessary spatial detail to the rainfall analyses over land. It is also available from NOAA/OAR/ESRL PSD, Boulder, Colorado, USA, web site (http://www.esrl.noaa.gov/psd/). For precipitation, Indian Meteorological Department (IMD) gridded rainfall dataset is also used (Rajeevan, M.et al, 2008). This is available from 1901 to 2014 [NCC gridded data product, Link: http://www.imdpune.gov.in/ publication/pub_index.html]. Observational data for SST are from Met Office Hadley Centre Sea Ice and sea Surface Temperature (HadISST) data set and discussed in detail by Rayner et al. (2003). It provides monthly globally-complete fields of SST and sea ice concentration on a 1 degree latitude-longitude grid from 1870 to date. It is also available from NCAS British Atmospheric Data Centre (http://badc.nerc.ac.uk/view/badc.nerc.ac.uk ATOM dataent hadisst).

The results in our analyses are similar with or without the trend removed, suggesting that the trend plays nominal role. Moreover, we find that the spatial patterns of ENSO are insensitive to using either a long time period (SST data) or short time period (rainfall data), in both models as well as observations. The same is also true for precipitation composites, suggesting different time period used in this study are not likely to qualitatively alter our results.

3. Results

3.1. Climatology of Indian Summer Monsoon Precipitation and Wind Fields (JJA):

The climatology of precipitation and local wind fields at the 200mb and 850mb level during JJA is presented in Fig 2. Results from the observations (top row), one typical high top model (HadGEM2-CC) (middle row) and one typical low top model (CCSM4) (bottom row) are presented. The common period of analyses between the observations and models is 1979 to 2005.

The climatology of precipitation (left) suggests more rainfall occurs in the Western coast of South India and Central North East India in observations as well as in models. It also agrees with Jourdain et al (2013) that used JJAS to derive a climatology.

The wind fields can give an indication of the location of divergence and convergence. The CNE is the region, located around the Inter Tropical Convergence Zone (ITCZ) ~20-30 °N during summer, can be considered as a merging point of both Walker circulation and regional Hadley circulation (Gill 1980, Goswami 1994, Webster et al 1998). The superposition of Hadley and Walker cells in the CNE region is captured well in terms of 200 mb wind (middle column). Around the 30 °N mean position, there is an anticyclone in observation as well as in models. The wind further south of that anticyclone is easterly and further north is westerly, as expected. Such anticyclonic air movement suggests a high pressure area and divergence of wind at this level. High pressure at 200mb will usually indicate a convergence of wind pattern in the 850mb level. A region of convergence is noticed around the CNE region at 850mb wind in the observations as well as in models (right column). (Streamlines are not shown when the 850mb surface cuts through the orography). As the anticyclonic movement at 200 mb is clearly distinguished in the streamline plot of winds, we present these types of plots throughout. However, in a supplementary figure (Fig S1), the same plot of wind is shown in vector form.

3.2. Correlation Analysis (JJA): ENSO and ISM

3.2.1. Teleconnection in Observations, HadGM2-CC and CCSM4

Although the observed negative correlation between El Niño SSTAs and ISM rainfall is well known, the correlation analysis suggests that not all regions in India are influenced (Fig. 3). The CNE and hilly regions, and parts of the East Peninsular region, show negative correlation between rainfall and the SSTAs of the Canonical region and region A. The CNE is the region located around the Inter Tropical Convergence Zone (ITCZ) ~20-28 °N during JJA, and acts as a merging point of both the Hadley and Walker circulations. Bollasina et al. (2011) identified a region in the CNE (CI in Fig1, bottom), that showed a significant decreasing trend during the 2nd half of the last century. Goswami et al. (2006) also identified similar region (CII in Fig 1, bottom), even when covering that box to the east of the Peninsular.

Using the EMI index, the observed correlation shows an opposite sign to that from the classical relationship around Central India. In other regions, correlations are weak.

For the first of the two CMIP5 models highlighted, HadGM2-CC**,** week negative correlations around the CNE are captured between the rainfall and the canonical/region A SSTAs but with the pattern shifted southwards. In the Peninsular region, the model fails to capture any teleconnection. For the EMI, no correlations are evident in HadGEM2-CC.

For CCSM4, there are biases in correlations in the north-west region for Canonical/region A SSTAs. Some correspondence with the observed teleconnection is evident around the eastern Bay of Bengal and there are slight indications of correlations in the Hilly region. The observed signal in EMI-rainfall correlation is again not captured. All three spatial patterns are very similar and thus CCSM4 fails to distinguish between the different types of ENSO teleconnection.

3.2.2. Teleconnections in other CMIP5 models

To summarise the evaluation of all the CMIP5 models we adopt two simple criteria and examine the teleconnections to the different SST regions, based in Fig.3.

- **CNE**- In the Central North East (CNE) and Hilly regions: more rainfall during La Niña and less during El Niño. It is marked by CI in Fig.1 (bottom).
- **PEN-** In Parts of the Eastern Peninsular Region: more rainfall during La Niña and less during El Niño. PEN region is south of CI region, that covers CII region (Fig. 1, bottom). The effects of both the regions CEN and PEN are considered in CII.

Table 2 (row 1-2) is formulated to show how good the CMIP5 models are in satisfying these criteria. It suggests that both teleconnections are captured by more than 50% models, irrespective of having high tops or low tops. Interestingly, the CNE criteria is satisfied by more than 80% model in the case of Canonical region SSTAs, but the ability to simulate teleconnections to region A is less well captured. Ashok and Yamagata (2009) suggested that the effectiveness of the current generation of coupled models in simulating ENSO Modoki features is lower than their ability to simulate conventional ENSO teleconnections. Moreover, from Table 2 (row 1-2), it is also seen that low top models are better at CNE, while high top models more frequently simulate the PEN teleconnection.

Apart from these main findings, we also identify that no model shows a positive rainfall signal in Central India associated with a positive EMI index, as is seen in the observations (Fig 3). Models closest in agreement with the observations are MPI-ESM-LR and GFDL-CM3. The model with the largest negative biases is IPSL-CM5A-LR, whereas, the model that shows very little in the way of rainfall teleconnections to India is MRI-CGCM3 [Supplementary Fig 2].

In observations, there is a positive signal over the monsoon trough area, and negative correlation to the south of it, using the EMI. To check this further with the work of Kumar et al. (2006) and Ashok et al. (2007), a different dataset is also used. This is gridded data of Rajeevan et al. (2008) and results for JJA are shown in Supplementary Fig. S3. Around the CNE and PEN region, a positive signature is again noticed. A negative region to the south of CNE, suggesting a dipolar kind of pattern is noticed for both EMI and Region A. Signatures identified in IMD data are in general weaker to that of GPCP. That is the reason the colour scale ranges are changed slightly for IMD data at lower values.

3.3. Compositing (JJA): ISM-ENSO teleconnections

El Niño and La Niña events are not mirror images of each other (Hoerling et al. 1997; Burgers and Stephenson 1999; Jin et al. 2003; Hannachi et al. 2003; An and Jin 2004; Monahan and

Dai 2004; Rodgers et al. 2004). There are not only asymmetries in spatial patterns (McPhaden and Zhang, 2009) and duration (Okumura and Deser, 2010) but the formation mechanisms also differ (Ohba and Ueda, 2009; Okumura et al, 2011). The lack of symmetry in the response to opposite phases of ENSO in North America is discussed in Hoerling et al. (1997), Gershunov and Barnett (1998), and Cayan et al. (1999). Hence it is useful to apply a compositing method, which can better isolate the differences between teleconnections during El Niño and La Niña.

Composites of ISM precipitation are calculated in canonical case, Modoki case and combined Canonical and Modoki situation. Results from one high top model (HadGEM2-CC) and one low top model (CCSM4) from CMIP5 are again compared with observations (GPCP). The CCSM4 model AMIP5 simulation is also included in comparison (Fig. 4 for El Niño and Fig. 5 for La Niña). Precipitation composites from the other CMIP5 and respective AMIP5 models are summarised in Table 2.

3.3.1. El Niño Precipitation Composites

The observed composite in Central North East (CNE) India shows a negative precipitation signature for all three El Niño situations, in agreement with the correlation analysis. However, positive precipitation in parts of India are also observed in all three types of events.

For the high top model, HadGM2-CC, there is an opposite signal in the west peninsular region to that from observations. Also, a negative bias is evident over the western central region for ENCM. The composite for the low top model, CCSM4, resembles the correlation map. The sign of precipitation around the west of India is wrong for ENC and ENM. In case of the CCSM4 AMIP5 simulation, the composite is different from the coupled case but still poorly compares to observations.

3.3.2. La Niña Precipitation Composites

In the observations, La Niña composites show a general excess of precipitation for all ENSO types. The Central North East (CNE) region shows more precipitation for LNC and LNM. Also, excess precipitation is noticed around the peninsular region for LNC and LNCM.

For HadGM2-CC, the comparison with observations is poor for LNM and LNCM though better for the LNC class. The CCSM4 composite is closer to observation for LNC and the AMIP5 version performs better than the CMIP5 version for LNM, whereas the opposite is true for LNC.

It is seen that composites of El Niño phases (Fig. 4) differ to that from respective La Niña phases (Fig.5) and they are not mirror images. The places where both the El Niño and La Niña phases do indicate opposite signals, strong correlations are found. CCSM4 performs better in both the correlation and compositing analysis.

This study focused on JJA being the active monsoon months. Using JJAS, we find there is not a single year for ENCM composites in observation and hence is difficult to compare model results with observations in the extended seasons. This is the main reason we carried out the analyses for JJA. However, we included the plots of precipitation for various categories of LN composites during JJAS in the supplementary section (Supplementary Fig. S4) to show that our major results are not affected.

3.3.3. Precipitation Composites in all Models

Again we summarise the compositing results for all the models in Table 2 by applying the criteria (CNE and PEN) to the precipitation composites. ENCM and LNCM situations are not considered and kept blank in Table 2 as no events are observed or discussed in that category.

Here we mainly focus on CNE, the region which is satisfied by more than half of the models (>50%), irrespective of high/low top or CMIP5/AMIP5. For El Niño, CMIP5 models are generally better at capturing the two teleconnections for in the case of models with a low top, while AMIP better capture the teleconnections in the high top case.

For La Niña, AMIP models are better than CMIP models in both the high and low top cases. It may indicates that the mechanism involved in La Niña teleconnections is different to that during El Niño (Okumura Y. M. et al. (2011), Ohba and Ueda (2009)).

However, because of the small sample sizes and the non-independence of different models, it is not expected that these findings are statistically significant.

ENSO years under each subcategory (ENC, LNC, ENM, LNM, ENCM, LNCM) as used for making composite analysis from observed SST and model simulations are also shown in Supplementary Table S1.

3.4. Compositing: SST

Could the model performance discussed above be a result of the patterns of SST associated with different types of El Niño and La Niña? To look at this we perform composite analysis of global SSTs based on the definitions of ENSO given in section 2.

The observations show the familiar patterns of Canonical and Modoki modes (Fig 6.) but we see here the pattern for the less-familiar mixed ENCM mode. HadGM2-CC overestimates the amplitude of both ENCM and ENM while underestimating the amplitude in the ENC case. This may explain why the teleconnection appears too strongly in the ENCM case and too weakly in the ENC case (Figs 3 and 4) in HadGEM2-CC but does not explain the lack of reproduction of the ENM teleconnection. CCSM4 however overestimates the magnitude of all three types of El Niño. The spatial patterns in the ENC and ENCM case are very similar, which might explain the similarity of the spatial patterns of rainfall teleconnections that are evident in this model. However, the Modoki mode seems quite distinct from the others, so that conclusion may not be valid. The La Niña SST composite for HadGM2-CC (Fig 7) is closer to observations in terms of the spatial pattern than CCSM4. But it should be mentioned that the spatial patterns of Canonical (LNC/ENC), Modoki (LNM/ENC) and Canonical Modoki (LNCM/ENCM) are distinct in almost all models.

Errors in the spatial patterns are also likely important. In general, there is no clear relationship between composite SST errors and the ability of models to reproduce the ISM-ENSO relationship.

3.5. Addressing Dynamical Mechanism.

To understand the underlying dynamical mechanisms for the teleconnections, various plots are presented using horizontal and vertical wind fields. (Fig. 8-13). To analyse the Walker Circulation, the vertical velocity of wind (omega) is considered along the whole longitudinal belt, averaged between 5ºN to 5ºS. The plots of omega (Fig. 8 and 9), wind at 200mb (Fig. 10 and 11) and wind at 850mb (Fig. 12 and 13) show changes in the Walker Circulation cells and associated divergence and convergence of wind around the Indian subcontinent. As vertical wind field is missing for HadGEM-CC, we presented results from HadGEM2-ES for omega.

Fig 8 and 9 show there is a descending motion of the Walker circulation from the east of Dateline (180°) for all phases of La Niña. The anomalous circulation is seen to be reversed if the focus is on El Niño events, irrespective of category. It indicates that the observations and the two chosen models agree with the known dynamics relating to the Walker Circulation teleconnection to India.

The results from other models that reproduce the climatology of ISM rainfall well (Jourdain et al, 2013) are also tested. Almost all the models agree with opposing nature of rising and descending motion of the Walker Circulation around east of the International Dateline in tropical Pacific in two opposite phases of the ENSO cycle (figures not shown). Apart from those chosen models it is also true for almost all the models.

Figure 10 and 11 show winds at 200mb in different ENSO phases. Figure 10 suggests that, for ENC and ENCM, there is an eastward wind further south of the CNE region. This direction is opposite to that of climatology, as shown in Fig 2. However the ENM wind response lacks consistency among models and observations. For ENM, a mid-latitude connection is seen for observation and HadGEM2. The regional Hadley circulation seems to have role during ENM events. For observations, only ENC shows a convergence of wind, which is responsible for suppression of rainfall during the El Niño phase, though it has moved further north from its usual location (with mean position at around 30N). In models, the cyclonic movement of winds to higher latitudes is also captured to some El Niño categories. Around the CNE region, the direction of winds seem to be consistent between models and observations.

For La Niña (Fig 11) in observations, the direction of wind is opposite to that of El Niño in the south of CNE region and follows the climatology. However, there are discrepancies between observation and models in different subcategories LNM has an anticyclonic pattern around 30 N in observations.

For 850mb wind, there are lots of differences between observations and model results (Fig 12 and 13). This is probably due to topography and models vary among each other in representing topography and local influences. However, there is one consistency around the CNE region where the change in direction of wind is clearly noticed for observed data. Moreover for models, almost all the cases suggest change in direction of wind around CNE.

3.6. Tropical Pacific SST and ISM in Central India.

The poor simulation of the Indian Monsoon in models has been noted in various studies (e.g., Sperber and Palmer, 1996; Gadgil and Sajani, 1998; Wang et al., 2004), however the multimodel ensemble (MME) was generally performs better than any single model (Krishnamurti et al., 1999; Doblas-Reyes et al., 2000; Palmer et al., 2000). An ensemble-mean SSTAs and ISM composites for concurrent JJAs are presented in Fig. 14, using nine models that reproduce the climatology of ISM rainfall well (Jourdain et al, 2013). The same nine models used here are ACCESS1-0, CCSM4, CanESM2, FGOALS-s2, HadGEM2-ES, HadGEM2-AO, NorESM1-ME, MIROC5 and FIO-ESM. The criteria of climatology of ISM rainfall, as used by Jourdain et al. (2013), refers to seasonal mean spatial rainfall. This captures the tropical Pacific SST anomalies and the associated precipitation anomalies around CNE region. The ensemble-mean teleconnection to the west Peninsular region is less well captured however. CNE region which is located around ITCZ can capture teleconnection associated with Walker circulation part, which may not be true for PEN. Results are similar using ensemble of all models.

The correspondence between tropical Pacific SST and ISM around central India in models and observation are depicted in Fig 15 (top panel). Two regions in the tropical Pacific are chosen, one in the East Pacific with latitude longitude band [10°S, 10°N, 140°W, 90°W] and the other in the Central Pacific [10°S, 10°N, 160°E, 150°W]. The box regions in India for ISM precipitation as defined by Bollasina et al (2011) and Goswami et al (2006) and shown as CI and CII in Fig. 1 are chosen. Composite precipitation anomaly in regions CI are plotted with respect to SST anomaly of the central Pacific (right) and east Pacific (left). ENSO Modoki (ENM/LNM), ENSO Canonical (ENC/LNC) and ENSO Canonical and Modoki (ENCM/LNCM) are shown by various colours, with observations by large same coloured diamond.

Fig 15 (top panel) suggests models agree with each other on the SST-ISM correlation around central India and that also matches with observation. The majority of models for El Niño composites show less precipitation and vice-versa for La Niña. This is more robust when the east Pacific SST (left panel, Fig.15) is considered than in the central Pacific case (right panel, Fig. 15).

The correspondence between local wind fields and the ISM around central India in models and observation are shown in Fig 15 (bottom panel). Zonal wind field (m/s) at 200mb (u 200) is considered for CI (left) and CII (right) regions at various ENSO phases, considering various CMIP5 models. It suggests that models agree with each other on the local wind field and ISM correlation around central India and that also matches with observation. The majority of models for El Niño (shown by red, pink and yellow) composites show less precipitation and vice-versa for La Niña (shown by blue, cyan and green). This is more robust for the CI region (left panel) than that for CII region (right panel). It is also noticed that during the El Niño, u 200 is positive, though negative for La Niña in almost all the models. That indicates a change in direction of the Walker circulation. Model results thus show consistencies, and are in accordance with the known mechanism of El Niño and La Niña and local wind directions of the Walker circulation. Moreover, it suggests that precipitation in the CNE region is generally negatively correlated with the local zonal eastward velocity at 200 mb, as is depicted by all models. A strong correspondence between precipitation and u 200 (significant up to 99% level) is noticed among models, when all the ENSO phases are considered together.

The results combining with discussion of section 3.5, thus indicate that the models can capture the Walker circulation and ISM rainfall around central India reasonably well.

4. Summary

Correlation studies between observed SST anomalies and ISM precipitation suggest not all regions in India are affected by ENSO. While half of the CMIP5 models capture rainfall teleconnections in central India, the Hilly region and in the Peninsular, half do not. Teleconnections associated with Canonical or east Pacific ENSO events are better captured than those for central Pacific or Modoki events. Around the central India and Hilly region, more than 80 % of models capture the sign of the precipitation teleconnection.

Using the compositing approach, it is again observed that not all regions of India are affected by ENSO and some regions even show the opposite signature from the well-known ENSO-ISM connection to all-India Rainfall. More than 50 % of models agree on the sign of the teleconnection around central India irrespective of model category (High Top or Low Top, CMIP5 or AMIP5). In general there is not much distinction when one considers high top and low top models separately. The teleconnection to the Peninsular region is not as well capture by models.

Compositing studies of SST suggests models usually capture tropical Pacific SST anomaly reasonably well. The model ensemble of tropical Pacific SST and ISM indicate a clear connection between the Walker circulation and ISM rainfall around central India, as is seen in observations.

This assessment of the fidelity of models should be useful in assessing future projections.

5. Acknowledgement.

This work is done under SAPRISE (South Asian Precipitation: A Seamless Assessment) project, NERC number NE/I022841/1. First author also acknowledges the funding from ReCoVER project, UK.

6. References.

Adler RF, Huffman GJ, Chang A, Ferraro R, Xie P, Janowiak J, Rudolf B, Schneider U, Curtis S, Bolvin D, Gruber A, Susskind J, Arkin P, Nelkin E (2003) The Version 2 Global Precipitation

Climatology Project (GPCP) Monthly Precipitation Analysis (1979-Present). J Hydrometeor 4: 1147-1167.

An S-I, Jin F-F (2004) Nonlinearity and Asymmetry of ENSO. J.Clim 17: 2400-2412.

Ashok K, Guan Z, Yamagata T (2001) Impact of Indian Ocean dipole on the relationship between the Indian Monsoon rainfall and ENSO. Geophys Res Lett 28 (23); 4499-4502.

Ashok K, Behera SK, Rao SA, Weng H, Yamagata T (2007) El Niño Modoki and its possible teleconnections. J Geophys Res 112: C11007. doi:10.1029/2006JC003798.

Ashok K, Yamagata T (2009) Climate change: The El Niño with a difference. Nature 461: 481-484. doi:10.1038/461481a.

Ashrit RG, Rupa Kumar K, Krishna Kumar K (2001) ENSO-monsoon relationships in a greenhouse warming scenario. Geophys Res Lett 28(9): 1727–1730.

Bellenger H, Guilyardi E, Leloup J, Lengaigne M, Vialard J (2014) ENSO representation in climate models: from CMIP3 to CMIP5. Clim Dyn 42: 1999-2018. doi:10.1007/s00382-013-1783-z

Bollasina MA, Ming Y, Ramaswamy V (2011) Anthropogenic Aerosols and the Weakening of the South Asian Summer Monsoon. Science 334: 502-505. doi: 10.1126/science.1204994.

Brown JN, McIntosh PC, Pook MJ, Risbey JS (2009) An investigation of the links between ENSO flavors and rainfall processes in Southeastern Australia. Mon Weather Rev 137: 3786–3795.

Burgers G, Stephenson DB (1999) The ‘‘normality’’ of El Niño. Geophys Res Lett 26: 1027–1030.

Cai W, Cowan T (2009) La Niña Modoki impacts Australia autumn rainfall variability. Geophys Res Lett 36: L12805. doi: 10.1029/2009GL037885.

Cayan DR, Redmond KT, Riddle LG (1999) ENSO and hydrologic extremes in the western United States. J Clim 12: 2881-2893.

Chang CP, Patrick H, Ju J (2001) Possible Roles of Atlantic Circulations on the Weakening Indian Monsoon Rainfall–ENSO Relationship. J. Clim 14: 2376-2380.

Chang CWJ, Hsu HH, Sheu WJ (2008) Interannual mode of sea level in South China Sea and the roles of El Niño Modoki. Geophys Res Lett 35: L03601. doi: 10.1029/2007GL032562.

Charlton-Perez AJ, Baldwin MP, Birner T, Black RX, Butler AH, Calvo N, Davis NA, Gerber EP, Gillett N, Hardman S, Kim J, Krüger K, Lee Y-Y, Manzini E, McDaniel BA, Polvani L, Reichler T, Shaw TA, Sigmond M, Son S-W, Toohey M, Wilcox L, Yoden S, Christiansen B, Lott F, Shindell D, Yukimoto S, Watanabe S (2013) On the lack of stratospheric dynamical variability in low-top versions of the CMIP5 models. J Geophys Res Atmos 118: 2494-2505. doi: 10.1002/jgrd.50125.

Doblas-Reyes FJ, Déqué M, Piedelieve J-P (2000) Multi-model spread and probabilistic seasonal forecasts in PROVOST. Q J R Meteorol Soc 126: 2035-2067.

Gadgil S, Sajani S (1998) Monsoon Precipitation in the AMIP run. Clim Dyn 14: 659-689.

Gershunov A, Barnett TP (1998) Interdecadal modulation of ENSO teleconnections. Bull Am Meteorol Soc 79: 1715–2725.

Gill A. E., 1980, Some simple solutions of heat induced tropical circulations. Q J R Meteorol. Soc 106: 447-462

Goswami BN (1994) Dynamical predictability of seasonal monsoon rainfall: Problems and prospects. Proc Indian Natl Sci Acad 60: 101-120.

Goswami BN, Venugopal V, Sengupta D, Madhusoodanan MS, Xavier PK (2006) Increasing Trend of Extreme Rain Events Over India in a Warming Environment. Science 314: 1442-1445. doi: 10.1126/science.1132027

Grimm AM (2003) The El Niño impact on summer monsoon in Brazil: Regional processes versus remote influences. J Clim 16: 263–280.

Grimm AM (2004) How do La Niña events disturb the summer monsoon system in Brazil? Clim Dyn, 22: 123–138.

Hannachi A, Stephenson DB, Sperber KR (2003) Probability-based methods for quantifying nonlinearity in ENSO. Clim Dyn 20: 241-256. doi:10.1007/s00382-003-0377-6.

Hill KJ, Taschetto AS, England MH (2009), South American rainfall impacts associated with inter-El Niño variations, Geophys Res Lett 36: L19702. doi: 10.1029/2009GL040164.

Hoerling MP, Kumar A, Zhong M (1997) El Niño, La Niña, and the nonlinearity of their teleconnections. J Clim 10: 1769-1786.

Huffman GJ, Adler RF, Bolvin DT, Gu G (2009) Improving the Global Precipitation Record: GPCP Version 2.1. Geophys Res Lett 36: L17808. doi: 10.1029/2009GL040000.

Hurrell JW, Hack JJ, Shea D, Caron JM, Rosinski J (2008) A New Sea Surface Temperature and Sea Ice Boundary Dataset for the Community Atmosphere Model. J Clim 21: 5145-5153. doi:10.1175/2008JCLI2292.1.

Hurwitz MM, Calvo N, Garfinkel CI, Butler AH, Ineson S, Cagnazzo C, Manzini E, Peña-Ortiz C (2014) Extra-tropical atmospheric response to ENSO in the CMIP5 Models. Clim Dyn 43: 3367-3376. doi 10.1007/s00382-014-2110-z.

IPCC, 2013: Climate Change 2013: The Physical Science Basis. Contribution of Working Group I to the Fifth Assessment Report of the Intergovernmental Panel on Climate Change

Stocker, T.F., D. Qin, G.K. Plattner, M. Tignor, S.K. Allen, J. Boschung, A. Nauels, Y. Xia, V. Bex and P.M. Midgley (eds.)]. Cambridge University Press, Cambridge, United Kingdom and New York, NY, USA, 1535 pp, doi:10.1017/CBO9781107415324.

Jin F-F, An S-I, Timmermann A, Zhao J (2003) Strong El Niño events and nonlinear dynamical heating Geophys Res Lett 30: 1120. doi: 10.1029/2002GL016356

Jourdain NC, Sen Gupta A, Taschetto AS, Ummenhofer CC, Moise AF, Ashok K (2013) The Indo-Australian monsoon and its relationship to ENSO and IOD in reanalysis data and the CMIP3/CMIP5 simulations. Clim Dyn 41 :3073–3102. doi 10.1007/s00382-013-1676-1

Kao H-Y, Yu J-Y (2009) Contrasting eastern-Pacific and central-Pacific types of El Niño. J Clim, 22: 615 – 632.

Krishnamurti TN, Kishtawal CM,.LaRow TE, Bachiochi DR, Zhang Z, Williford CE, Gadgil S, Surendran S (1999) Improved weather and seasonal climate forecasts from multi-model superensemble. Science 285: 1548–1550. doi:10.1126/science.285.5433.1548.

Kumar KK, Rajagopalan B, Cane MA (1999) On the weakening relationship between the Indian Monsoon and ENSO. Science 284 (5423): 2156-2159.

Kug J-S, Jin F-F, An S-I (2009) Two types of El Niño events: cold tongue El Niño and warm pool El Niño. J Clim 22:1499–1515.

Larkin NK, Harrison DE (2005) On the definition of El Niño and associated seasonal average U.S. weather anomalies. Geophys Res Lett 32: L13705. doi: 10.1029/ 2005GL022738.

Marathe S., Ashok K, Swapna P et al , 2015, Climate Dynamics, 45, DOI: 10.1007/s00382-015-2555-8,3527-3545.

Maity R, Kumar DN. (2006). Bayesian dynamic modelling for monthly Indian summer monsoon rainfall using El Niño–Southern Oscillation (ENSO) and Equatorial Indian Ocean Oscillation (EQUINOO). J Geophys Res 111: D07104.

Meyer PL. (1970). Introductory Probability and Statistical Applications, Addison-Wesley: Reading.

Mcphaden M, Zhang X (2009) Asymmetry in zonal phase propagation of ENSO sea surface temperature anomalies. Geophys Res Lett 36: L13703. doi: 10.1029/2009GL038774.

Monahan AH, Dai A (2004) The spatial and temporal structure of ENSO nonlinearity. J Clim 17: 3026-3036.

Ohba M, Ueda H (2009) Role of nonlinear atmospheric response to SST on the asymmetric transition process of ENSO. J. Clim 22:177-192.

Okumura YM, Deser C (2010) Asymmetry in the Duration of El Niño and La Niña. J Clim 23: 5826-5843. doi: 10.1175/2010JCLI3592.1

Okumura YM, Ohba M, Deser C, Ueda H (2011) A Proposed Mechanism for the Asymmetric Duration of El Niño and La Niña. J Clim 24: 3822–3829. doi: 10.1175/2011JCLI3999.1

Palmer TN, Brankovic C, Richardson DS (2000), A probability and decision-model analysis of PROBOST seasonal multi-model ensemble integrations, Q J R Meteorol Soc 126: 2013–2034. doi:10.1256/ smsqj.56702.

Population Reference Bureau, 2014. Publisher, Washington, DC 20009 US, 20 pp. http://www.prb.org/pdf14/2014-world-population-data-sheet_eng.pdf).

Rajeevan, M., Jyoti Bhate, A.K.Jaswal, 2008 : Analysis of variability and trends of extreme rainfall events over India using 104 years of gridded daily rainfall data, Geophysical Res. Letters, Vol.35, L18707, doi:10.1029/2008GL035143.

Ratnam VJ, Behera SK, Masumoto Y, Takahashi K, Yamagata T (2010) Pacific Ocean origin for the 2009 Indian summer monsoon failure. Geophys Res Lett 37: L07807, doi: 10.1029/2010GL042798.

Rayner NA, Parker DE, Horton EB, Folland CK, Alexander LV, Rowell DP, Kent EC, Kaplan A (2003) Global analyses of sea surface temperature, sea ice, and night marine air temperature since the late nineteenth century. J Geophys Res 108 (D14): 4407 10.1029/2002JD002670.

Rodgers KB, Friederichs P, Latif M (2004) Tropical Pacific decadal variability and its relation to decadal modulations of ENSO. J Clim 17: 3761-3774.

Roy I, Collins M (2014) On identifying the role of Sun and the El Niño Southern Oscillation on Indian Summer Monsoon Rainfall. Atmos Sci Let 16: 162-169. doi**:** 10.1002/asl2.547

Roy, I.; Tedeschi, R.G. Influence of ENSO on Regional Indian Summer Monsoon Precipitation—Local Atmospheric Influences or Remote Influence from Pacific. *Atmosphere* **2016**, *7*, 25.

Ropelewski CF, Halpert MS (1987) Global and regional scale precipitation patterns associated with the El Niño-Southern Oscillation. Mon Weather Rev 115: 1606–1626.

Sperber KR, Palmer TN (1996) Interannual Tropical Rainfall variability in General Circulation Model simulations Associated with the Atmospheric Model Intercomparison Project. J. Clim 9: 2722-2750.

Taylor KE, Stouffer RJ, Meehl GA (2012) An overview of CMIP5 and the experimental design. Bull Am Met Soc 93:485–498. doi:10.1175/BAMS-D-11-00094.1

Taschetto AS, England MH. (2009). El Niño Modoki impacts on Australian rainfall. J Clim 22: 3167–3174.

Tedeschi RG, Cavalcanti IFA, Grimm AM (2013) Influences of two types of ENSO on South American Precipitation. Int J Climatol. 33: 1382–1400. doi: 10.1002/joc.3519

Tedeschi RG, Collins M (2015) The influence of ENSO on South American precipitation during austral summer and autumn in observations and models. Int J Climatol. Doi: 10.1002/joc.4371

Trenberth KE, Caron JM, Stepaniak DP, Worley S (2002). Evolution of El Niño-Southern Oscillation and global atmospheric surface temperatures. J Geophys Res 107(D8): 4065, doi: 10.1029/2000JD000298.

Trenberth KE, Hurrell JW, Stepaniak DP (2006), The Asian monsoon: Global perspective, in The Asian Monsoon, pp. 67–87, Springer, New York.

Turner AG, Inness PM, Slingo JM (2005) The role of the basic state in the ENSO-Monsoon relationship and implications for predictability. Q J R Meteorol Soc 131 (607): 781–804.

Wang B, Kanf I-S, Lee J-Y (2004). Ensemble Simulations of Asian–Australian Monsoon Variability by 11 AGCMs. J Clim 17: 803-818.

Webster PJ, Magana VO,.Palmer TN, Shukla J, Tomas RA, Yanai M, Yasunari T (1998), Monsoons: Processes, predictability, and the prospects for prediction. J Geophys Res 103: 14451-14510.

Weng H, Ashok K, Behera SK, Rao SA, Yamagata T (2007) Impacts of recent El Niño Modoki on dry/wet conditions in the Pacific rim during boreal summer. Clim Dyn 29: 113–129. doi:10.1007/s00382-007-0234-0.

Weng H, Behera SK, Yamagata T (2009) Anomalous winter climate conditions in Pacific rim during recent El Niño Modoki and El Niño events. Clim Dyn 32: 663–674. doi: 10.1007/s00382-008-0394-6.

Yim S-Y, Wang B, Liu J, Wu Z (2014) A comparison of regional monsoon variability using monsoon indices. Clim Dyn 43: 1423-1437. doi: 10.1007/s00382-013-1956-9.

Yeh S, Kug J, Dewitte B, Kwon M, Kirtman B, Jin F (2009) El Niño in a changing climate Nature 461: 511-514. doi: 10.1038/nature08316.

Table 1. CMIP5 modelling centres and model names for coupled historical and atmosphere-only AMIP5. Models with high tops (H) and low tops (L) are indicated in the right hand column.

Model Centre	Model Type		High Top (H) /Low Top (L)
	CMIP5	AMIP5	
CSIRO-BOM, Australia	ACCESS1.0 ACCESS1.3	ACCESS1.0 ACCESS1.3	L L
BCC, China	BCC-CSM1.1 BCC-CSM1.1(m)	BCC-CSM1.1 BCC-CSM1.1(m)	L L
GCESS, China	BNU-ESM	BNU-ESM	L
CCCMA, Canada	CanESM2	CanAM4	L
NCAR, USA	CCSM4	CCSM4	L
CMCC, Italy	CMCC-CM	CMCC-CM	L
CNRM-CERFACS, France	CNRM-CM5	CNRM-CM5	L
CSIRO-QCCCE, Australia	CSIRO-Mk3.6.0	CSIRO-Mk3.6.0	L
LASG-CESS, China	FGOALS-g2	FGOALS-g2	L
LASG-IAP, China	FGOALS-s2	FGOALS-s2	L
INM, Russia	INM-CM4	INM-CM4	L
MIROC, Japan	MIROC5	MIROC5	L
NCC, Norway	NorESM1-ME	NorESM1-ME	L
NOAA-GFDL, USA	GFDL-CM3	GFDL-CM3	H
MOHC, England	HadGEM2-CC	HadGEM2-A	H
NASA-GISS, USA	GISS-E2-R	GISS-E2-R	H
IPSL, France	IPSL-CM5A-LR IPSL-CM5A-MR	IPSL-CM5A-LR IPSL-CM5A-MR	H H
MPI-M, Germany	MPI-ESM-LR MPI-ESM-MR	MPI-ESM-LR MPI-ESM-MR	H H
MRI, Japan	MRI-CGCM3	MRI-CGCM3	H

Table 2: Percentage of models able to reproduce the sign of ENSO teleconnections (see text). The first two rows are derived from a correlation analysis and the remaining table relates to an analysis of composite patterns. A blank in any cell means no events are observed or discussed in that category. For the first two rows, the number of models corresponding to the percentages are indicated (e/g/ 13/15). Low and High refer to models with low tops and high tops respectively.

	SSTA		**Canonical Region**	**Region A**
Correlation (Precipitation vs. SST) **CMIP models**	**CNE** CNE and Hilly-more(less) rain in La Niña (El Niño)	Low High	87 %, 13/15 83 %, 7/8	80 %, 12/15 66 %, 5/8
	PEN Parts E. Peninsular- more (less) rain in La Niña (El Niño)	Low High	47 %, 7/15 66 %, 5/8	53 %, 8/15 66 %, 5/8

			EN (%)			**LN (%)**		
			ENC	**ENCM**	**ENM**	**LNC**	**LNCM**	**LNM**
Precipitation Composites	**CNE** CNE and Hilly-more(less) rain in LN(EN)	Low CMIP	87		66	60		73
		Low AMIP	66		53	80		80
		High CMIP	62		50	62		75
		High AMIP	100		60	87		75
	PEN Parts E. Peninsular- more (less) rain in LN(EN)	Low CMIP	40		27	33		40
		Low AMIP	47		60	47		33
		High CMIP	37		37	12		50
		High AMIP	75		12	62		75

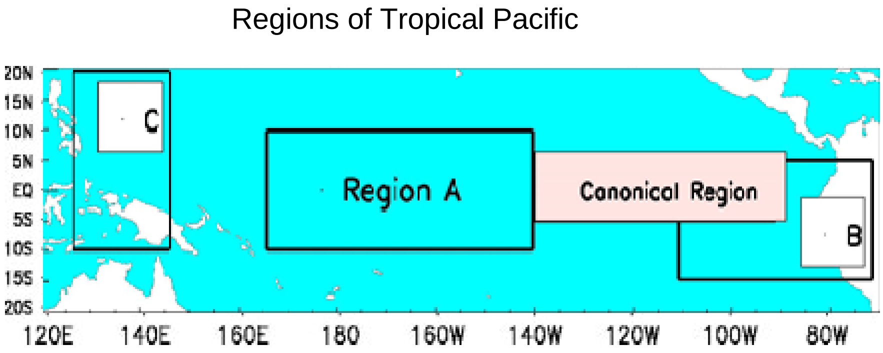

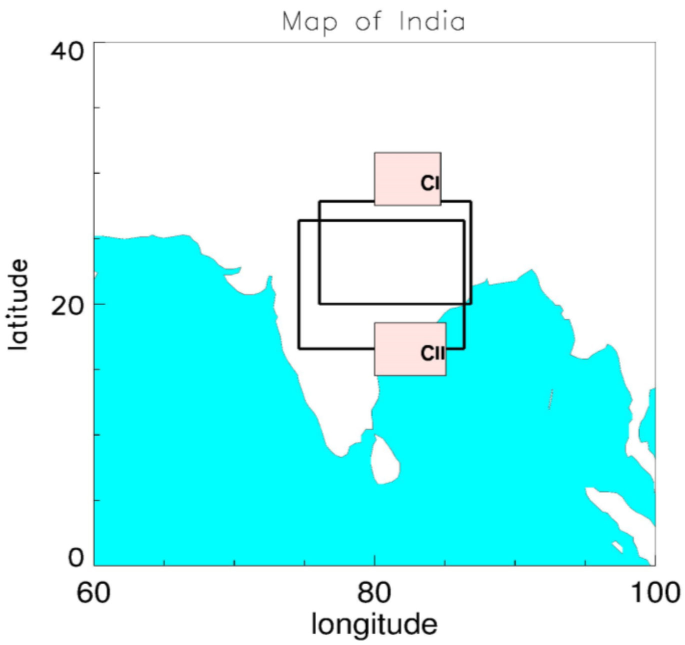

Fig.1: Various regions of Tropical Pacific are used to define different types of ENSO using SST anomalies (Top). Map of India with CI and CII regions marked with appropriate boundaries (bottom).

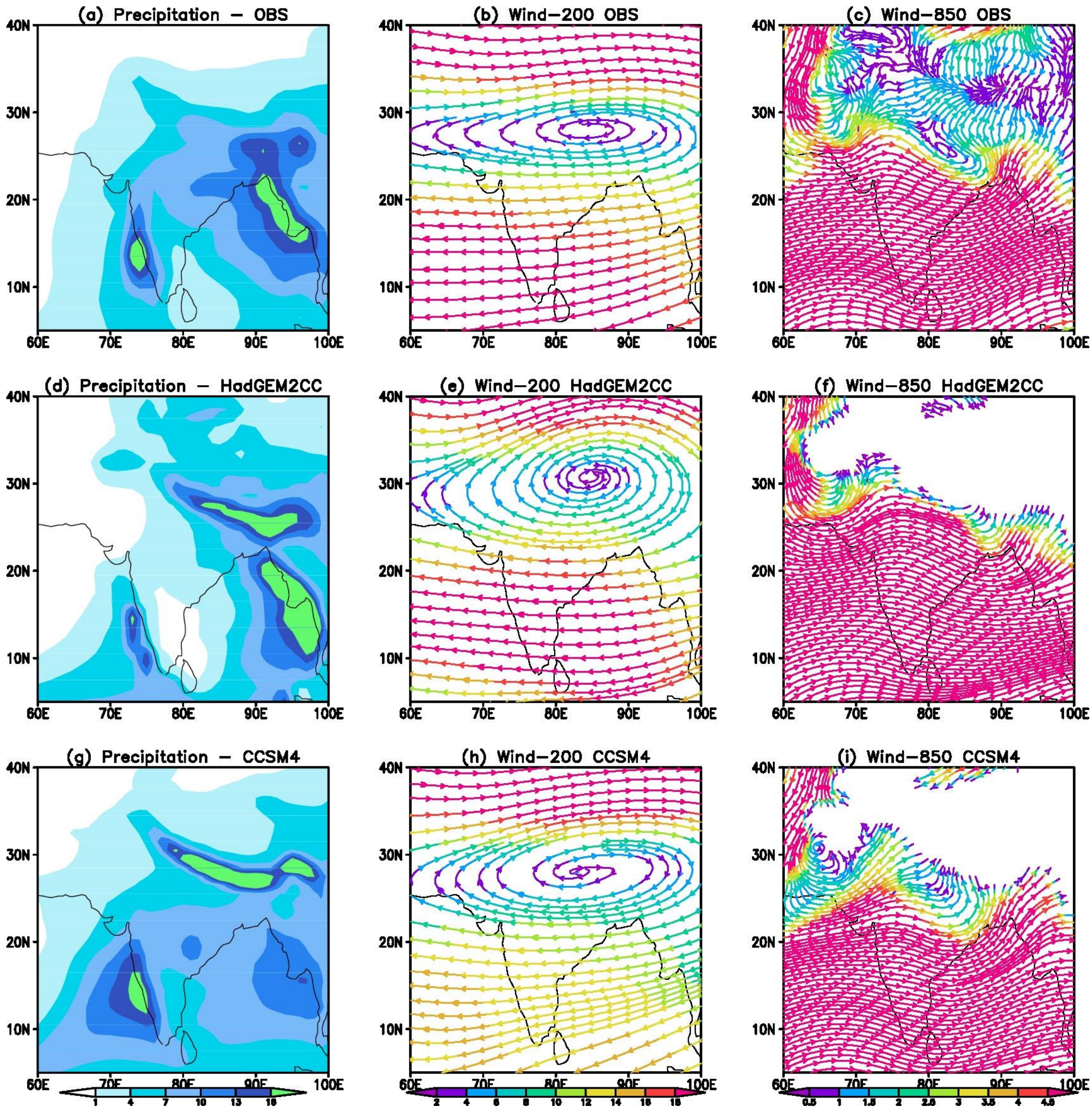

Fig. 2. The climatology of precipitation (left) in mm/day and wind fields at 200mb (middle) and 850mb level (right) in m/s during JJA for period 1979 to 2005. The top row for observed data, middle row for one typical high top model (HadGEM2-CC) and the bottom row for a typical low top model (CCSM4).

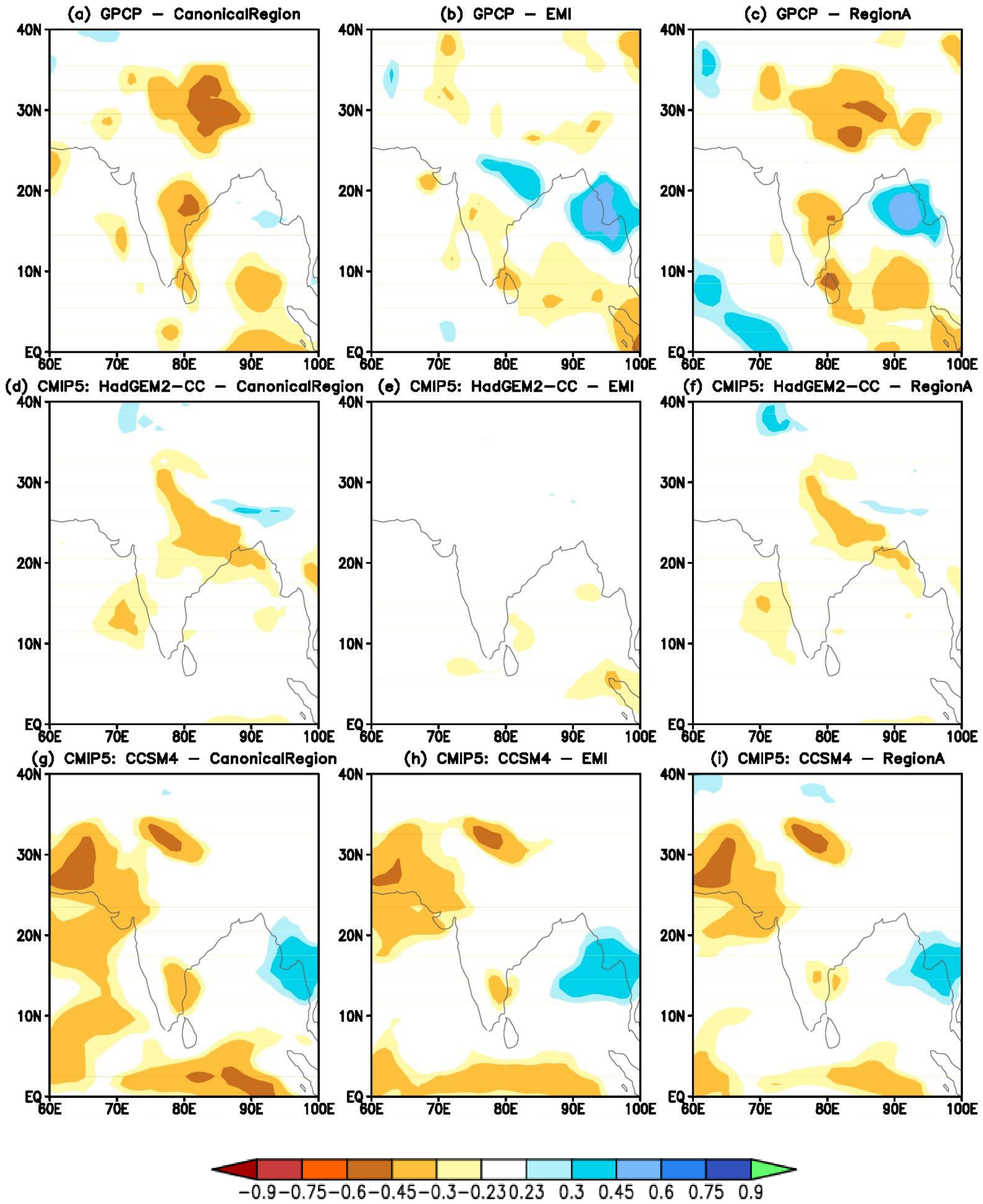

Fig.3. Correlation between Indian Summer Monsoon (JJA) rainfalls (mm/day) with the canonical region SST (°C) anomalies (left column), the El Niño Modoki Index (middle column) and region A SST anomalies (right column). The top row is computed from observation (GPCP) and correlations and shown for two typical models, one high top (HadGEM2-CC – middle row) and one low top (CCCM4 – bottom row). The level of significance is tested using Student's t-test and coloured regions indicate significant level of greater than 90%.

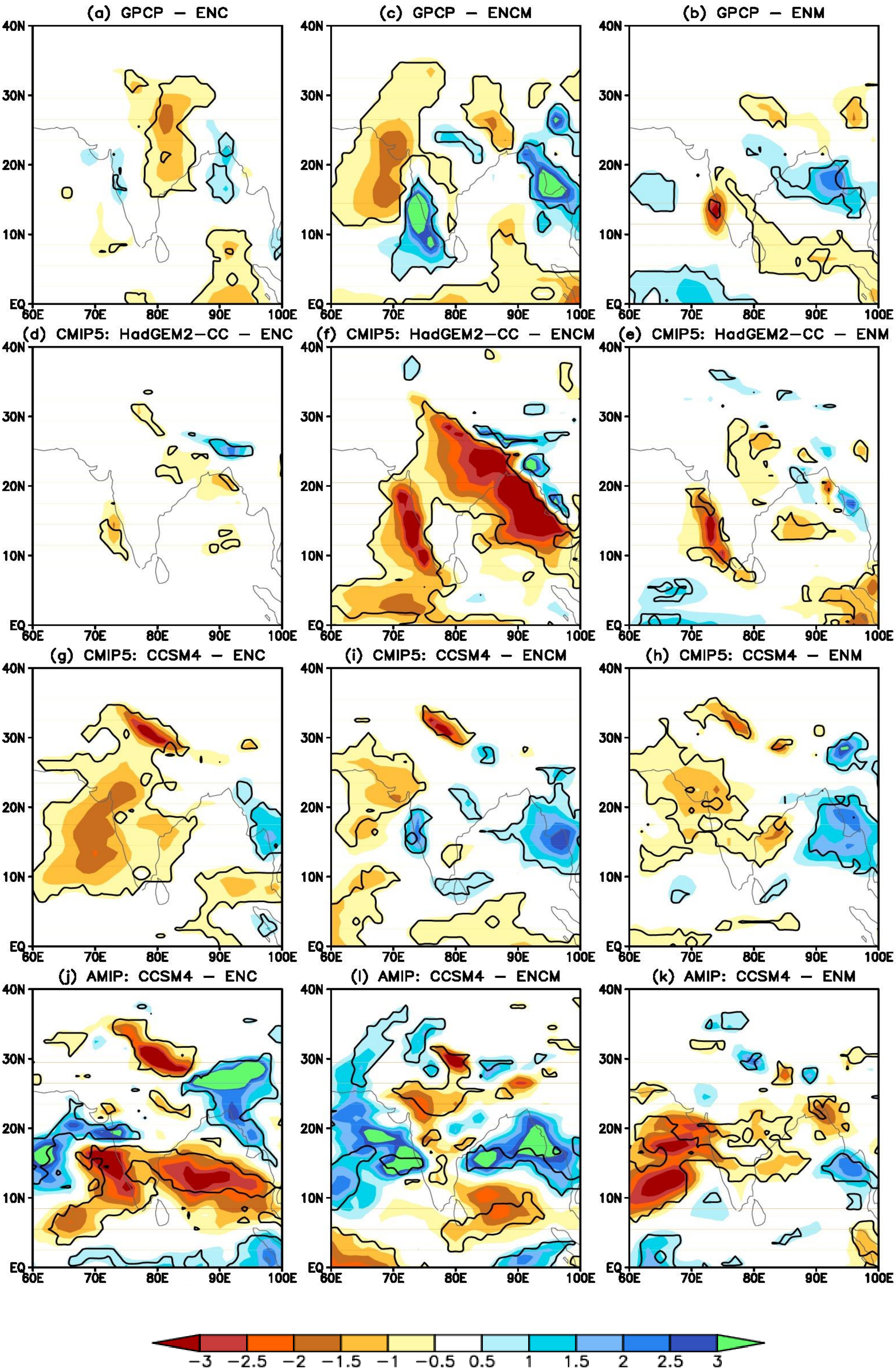
(a) GPCP – ENC
(c) GPCP – ENCM
(b) GPCP – ENM
(d) CMIP5: HadGEM2–CC – ENC
(f) CMIP5: HadGEM2–CC – ENCM
(e) CMIP5: HadGEM2–CC – ENM
(g) CMIP5: CCSM4 – ENC
(i) CMIP5: CCSM4 – ENCM
(h) CMIP5: CCSM4 – ENM
(j) AMIP: CCSM4 – ENC
(l) AMIP: CCSM4 – ENCM
(k) AMIP: CCSM4 – ENM
40N
30N
20N
10N
EQ
60E
70E
80E
90E
100E
–3 –2.5 –2 –1.5 –1 –0.5 0.5 1 1.5 2 2.5 3

Fig.4. Precipitation (JJA) Composites (mm/day) for El Niño, CMIP5 vs AMIP5. Comparing one typical high top model (HadGEM2-CC) and one typical low top CMIP5 model (CCSM4) with observation (GPCP). Observations are shown in the top panel. Bottom panel, AMIP Low Top CCSM4 model. Right panel is for composites in ENM years, left for ENC years and the middle for ENCM years.

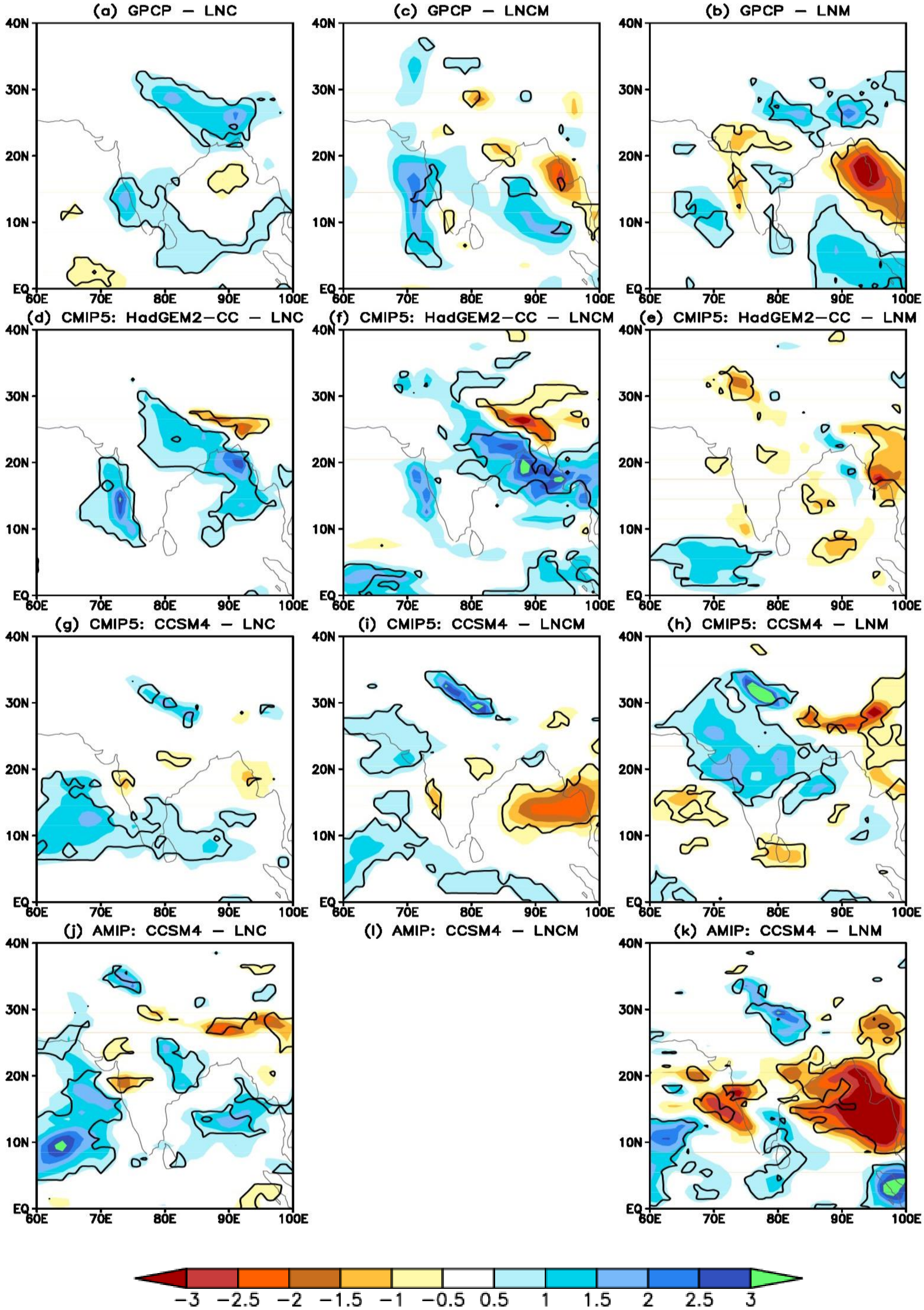

Fig.5. As Fig. 4 for La Niña composites.

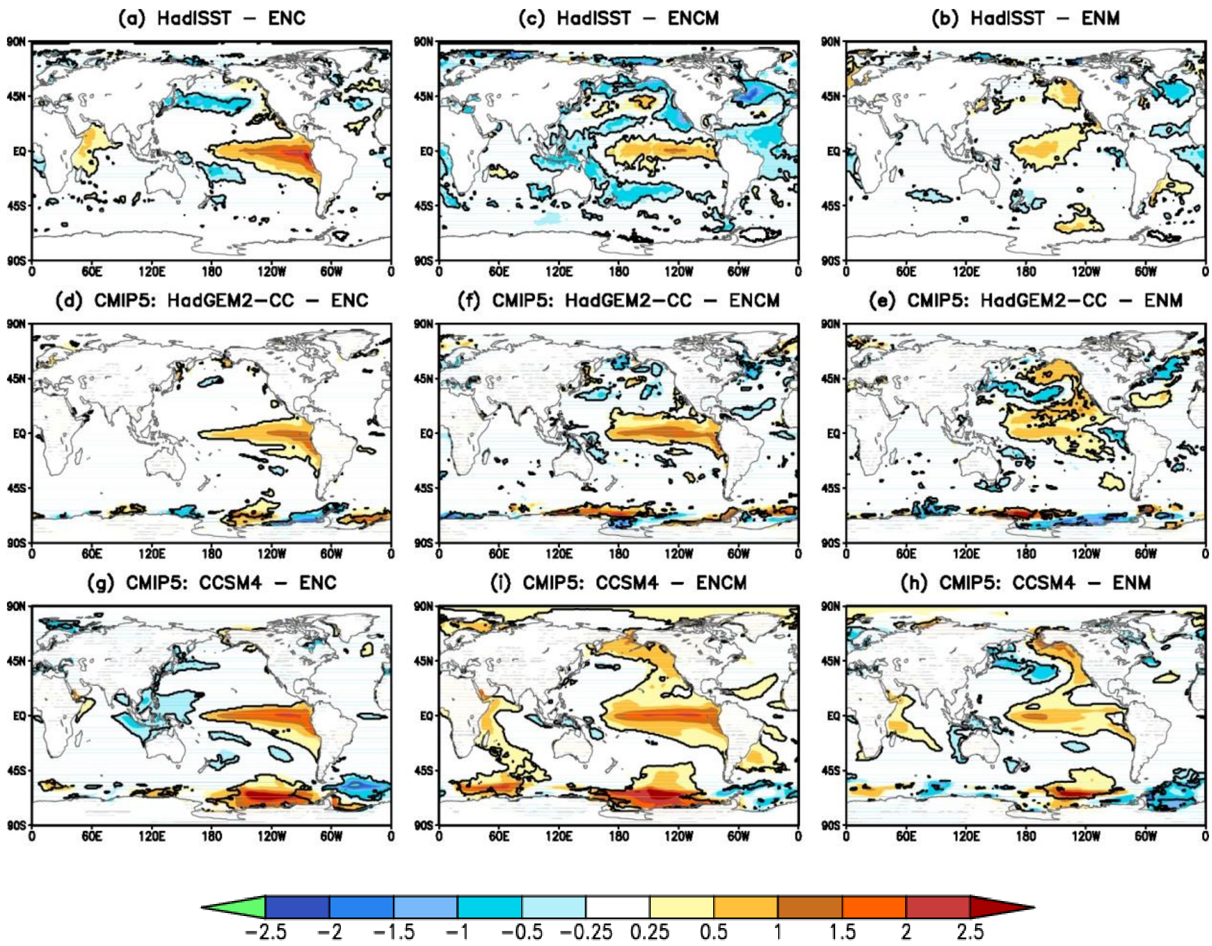

Fig. 6. El Niño composites during JJA for SSTA (°C) comparing one typical high top (HadGEM2-CC) and low top model (CCSM4) with observations (HadISST). Right panel is for composites on SST anomalies for ENM years, left for ENC years and the middle one for ENCM years.

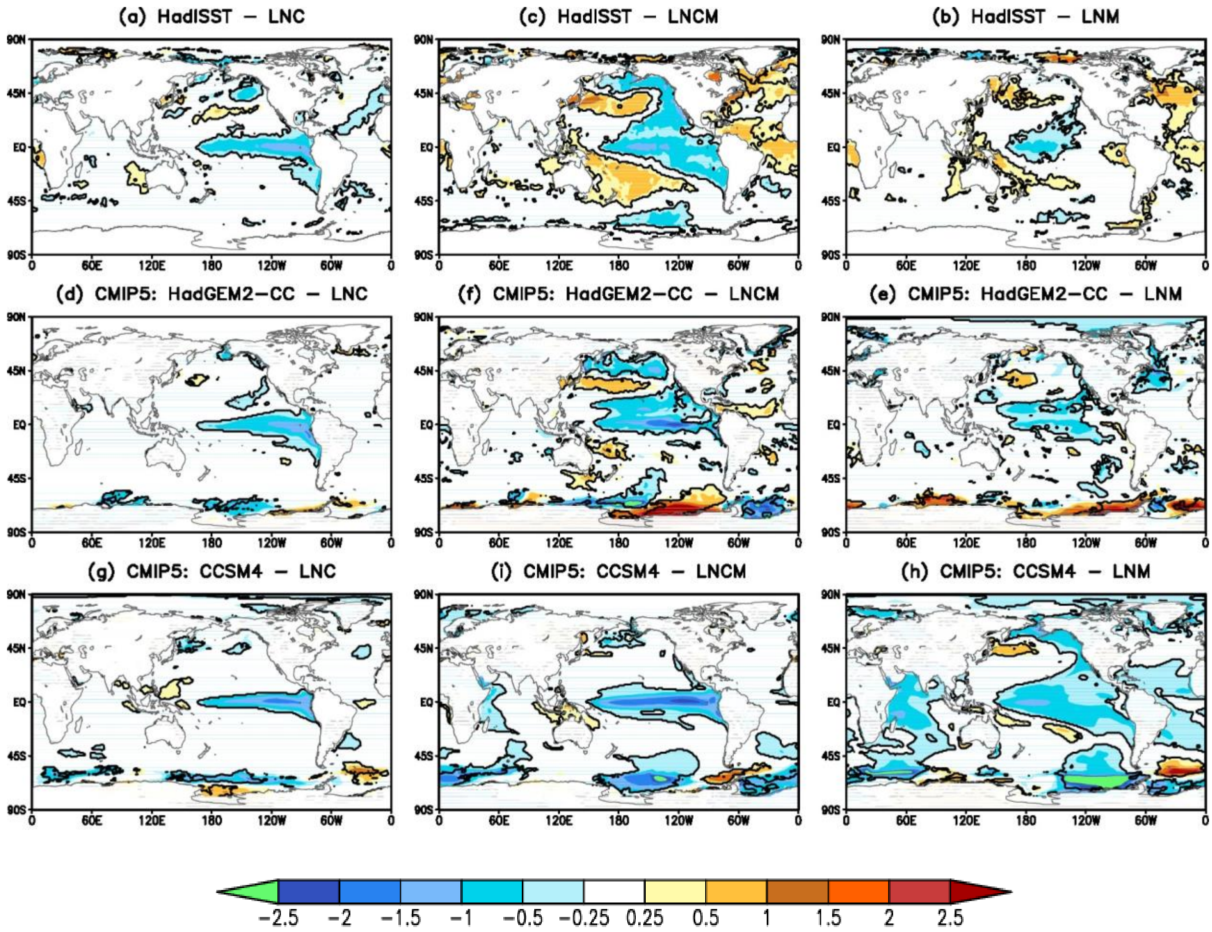

Fig. 7. As in Fig. 6 for La Niña.

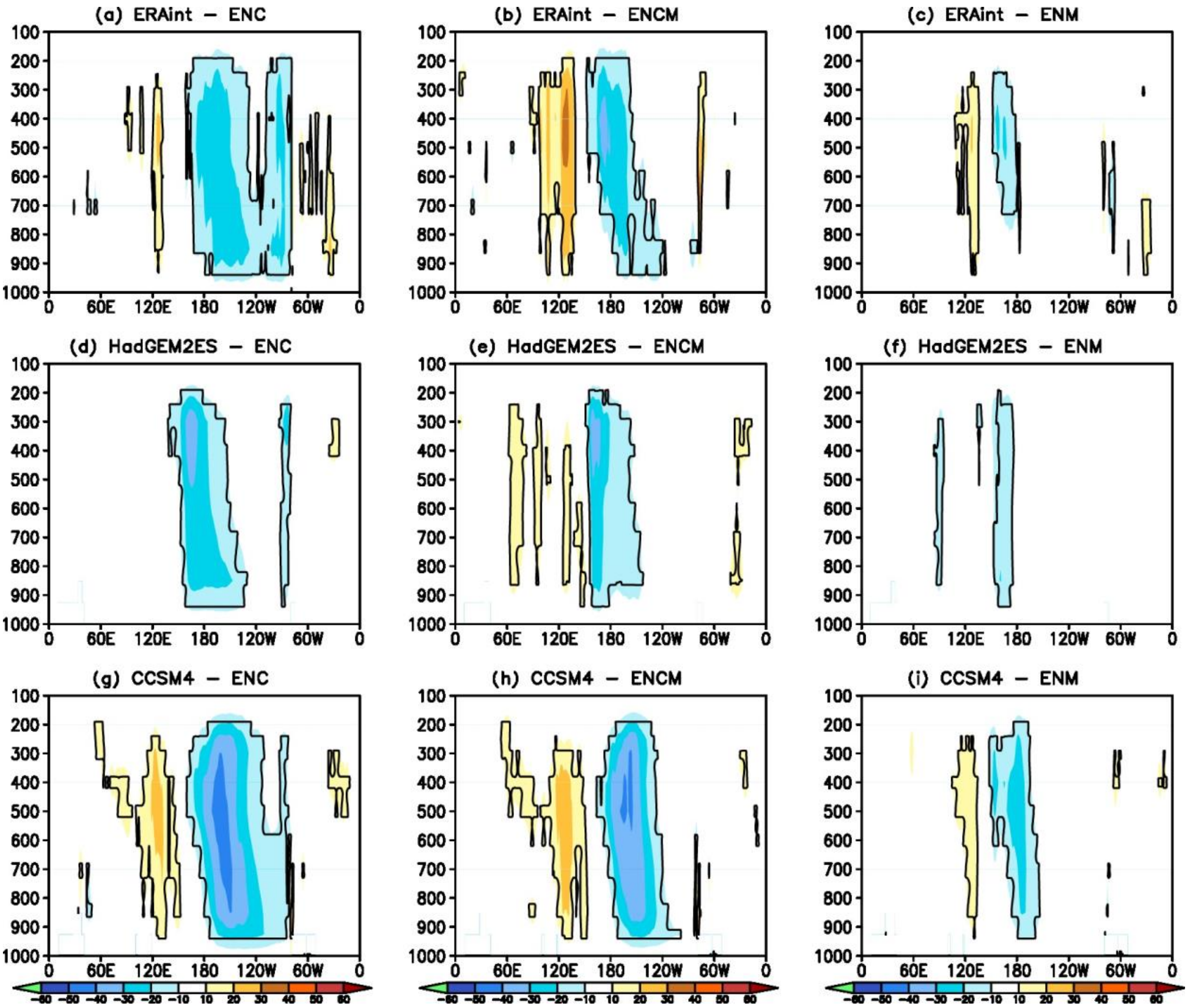

Fig. 8. El Niño composites during JJA for wind vertical velocity omega (m/s) comparing one typical high top (HadGEM2-CC) and low top model (CCSM4) with observations (ERA Interim). Right panel is for composites on omega anomalies for ENM years, left for ENC years and the middle one for ENCM years.

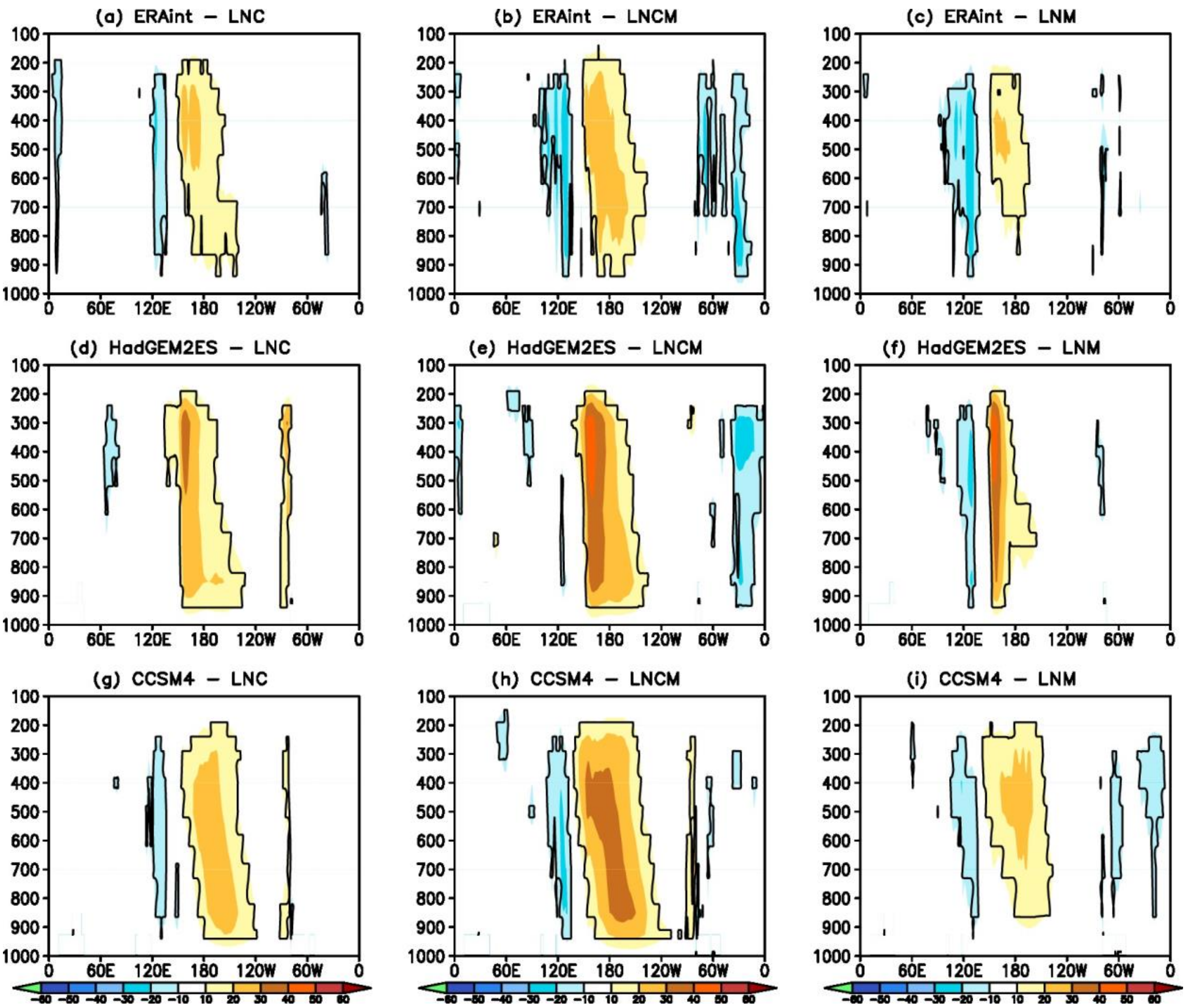

Fig. 9. As in Fig. 8 for La Niña.

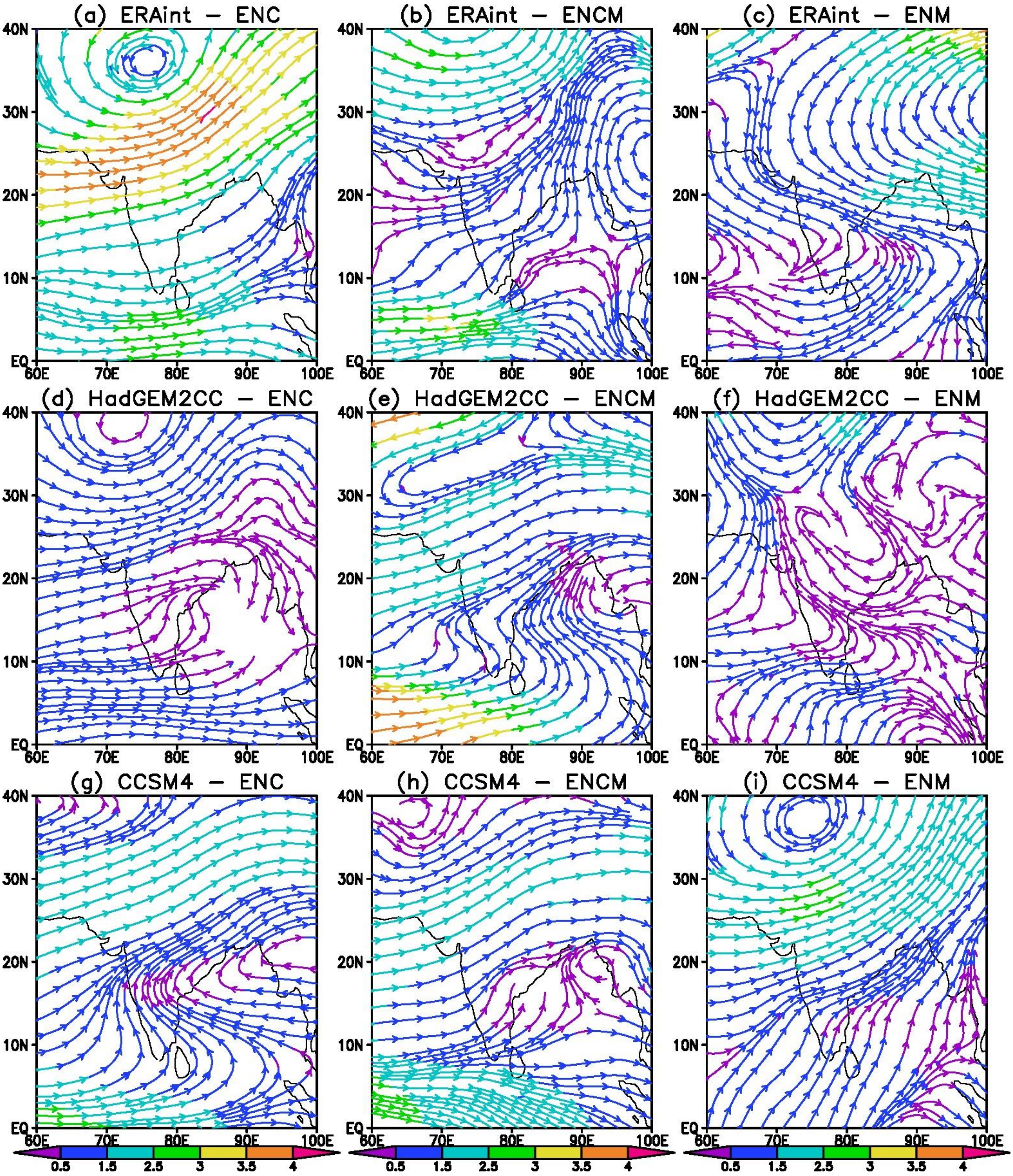

Fig. 10. El Niño composites during JJA for wind at 200 mb (m/s) comparing one typical high top (HadGEM2-CC) and low top model (CCSM4) with observations (ERA Interim). Right panel is for composites on wind 200mb anomalies for ENM years, left for ENC years and the middle one for ENCM years.

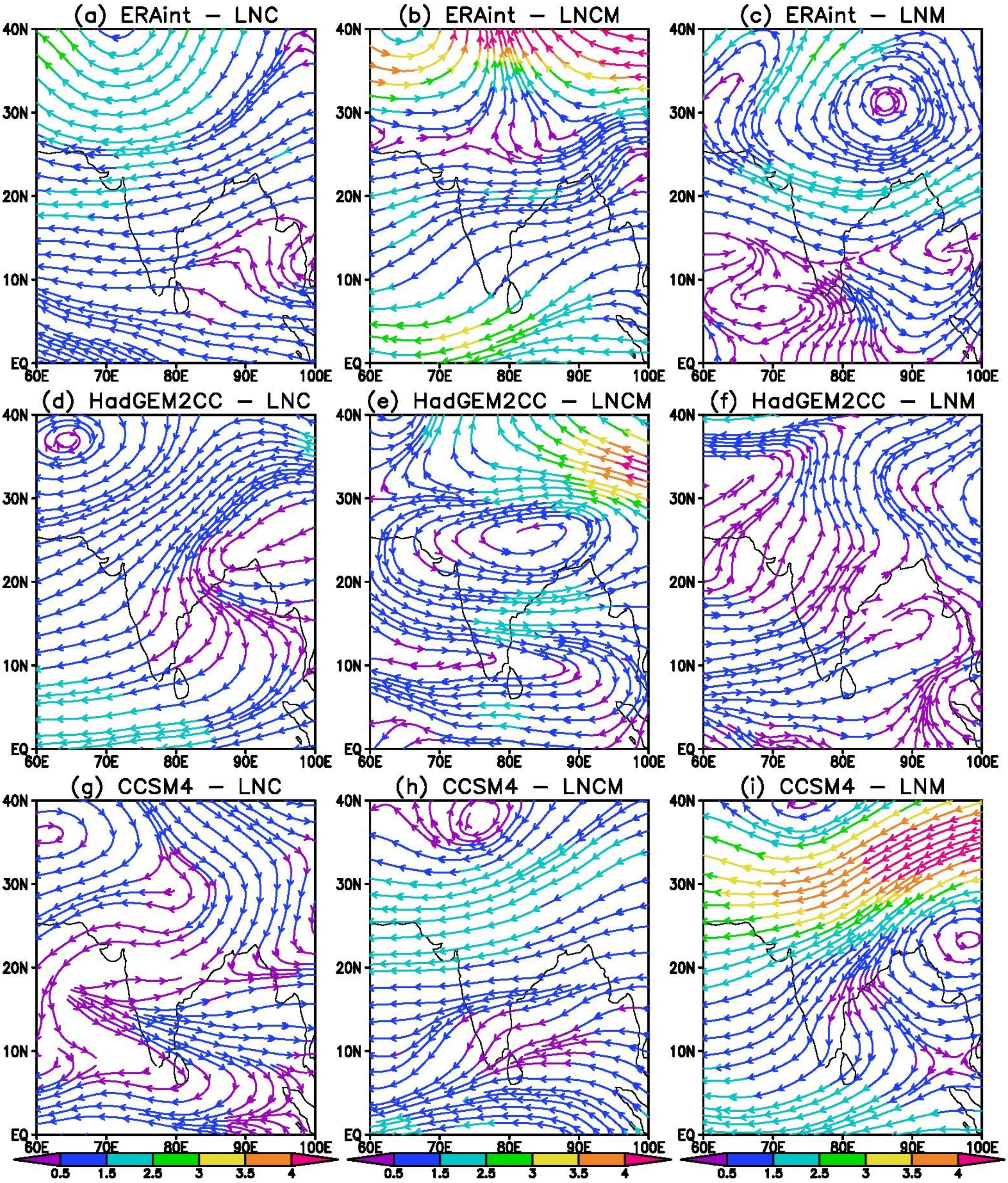

Fig. 11. As in Fig. 10 for La Niña.

.

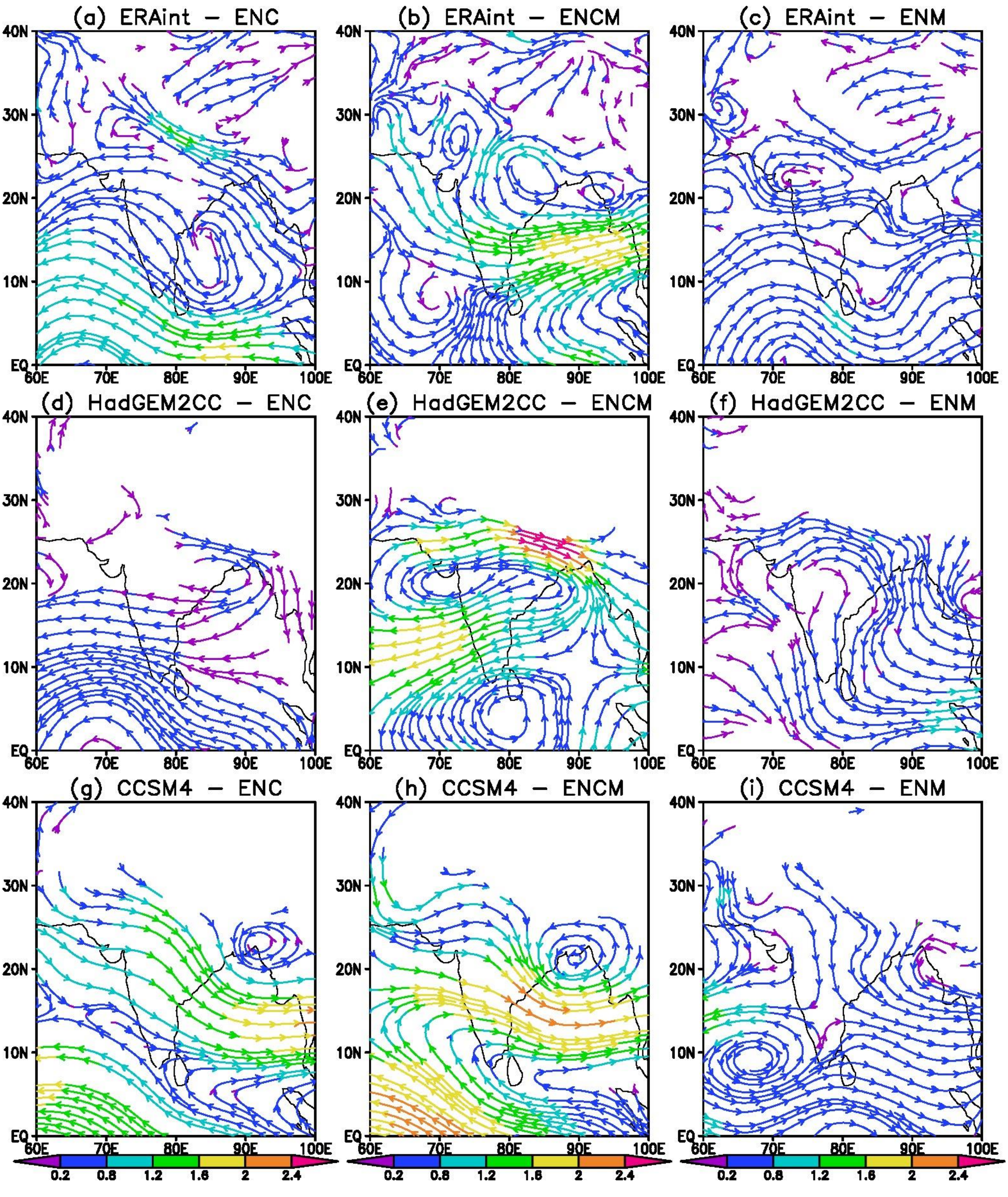

Fig. 12. El Niño composites during JJA for wind at 850 mb (m/s) comparing one typical high top (HadGEM2-CC) and low top model (CCSM4) with observations (ERA Interim). Right panel is for composites on wind 850mb anomalies for ENM years, left for ENC years and the middle one for ENCM years.

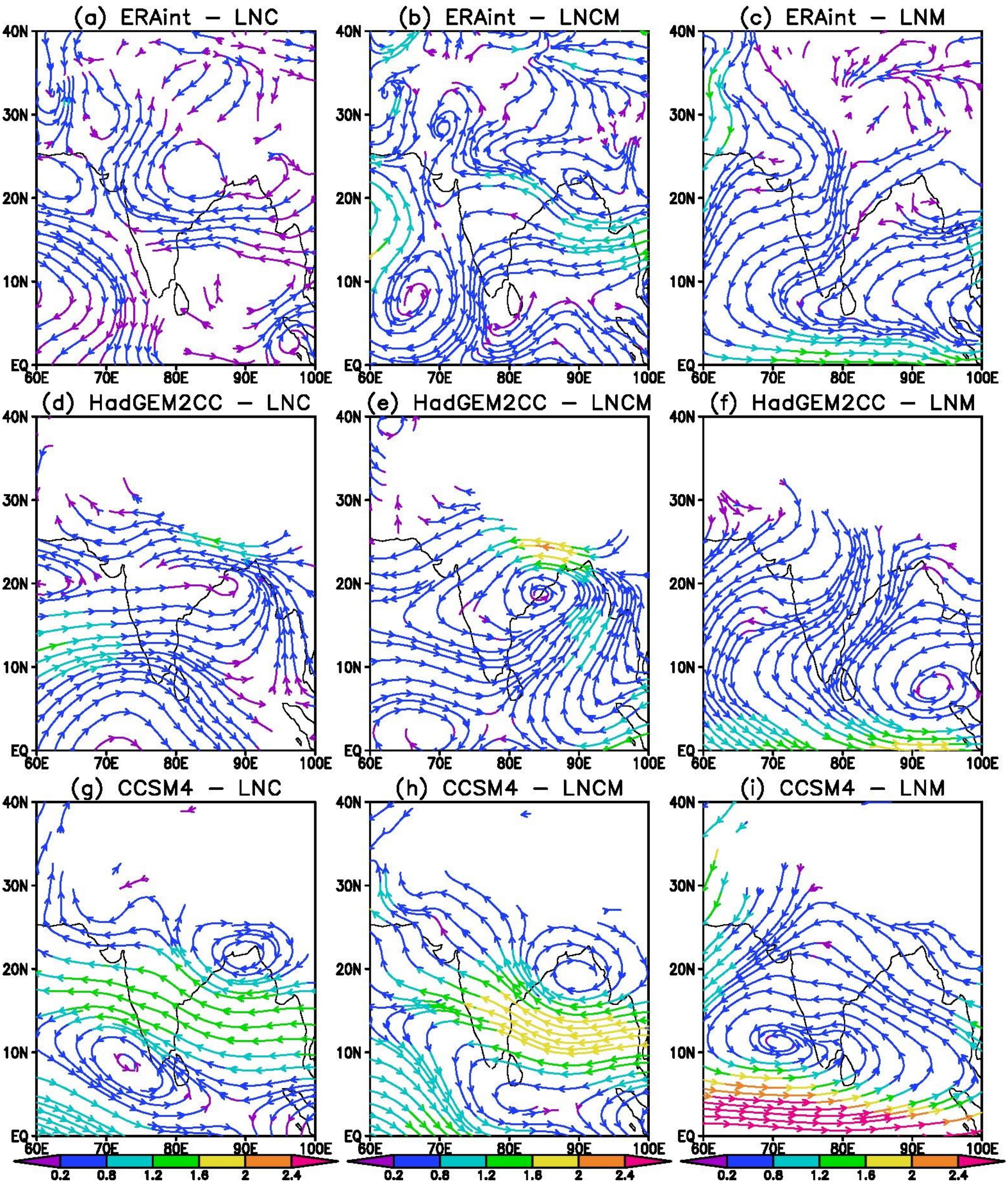

Fig. 13. As in Fig. 12 for La Niña.

Precipitation (JJA) - Ensemble Mean

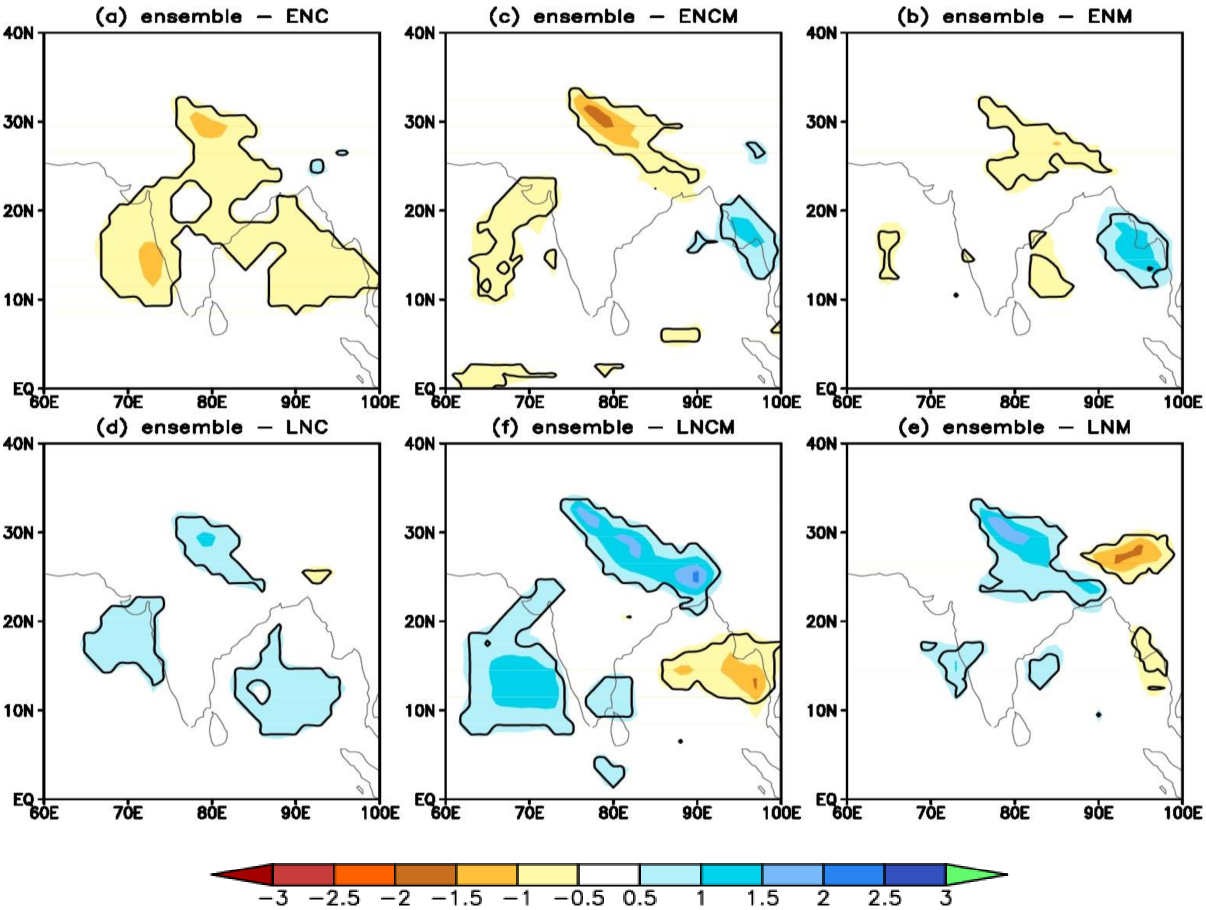

SST (JJA) - Ensemble Mean

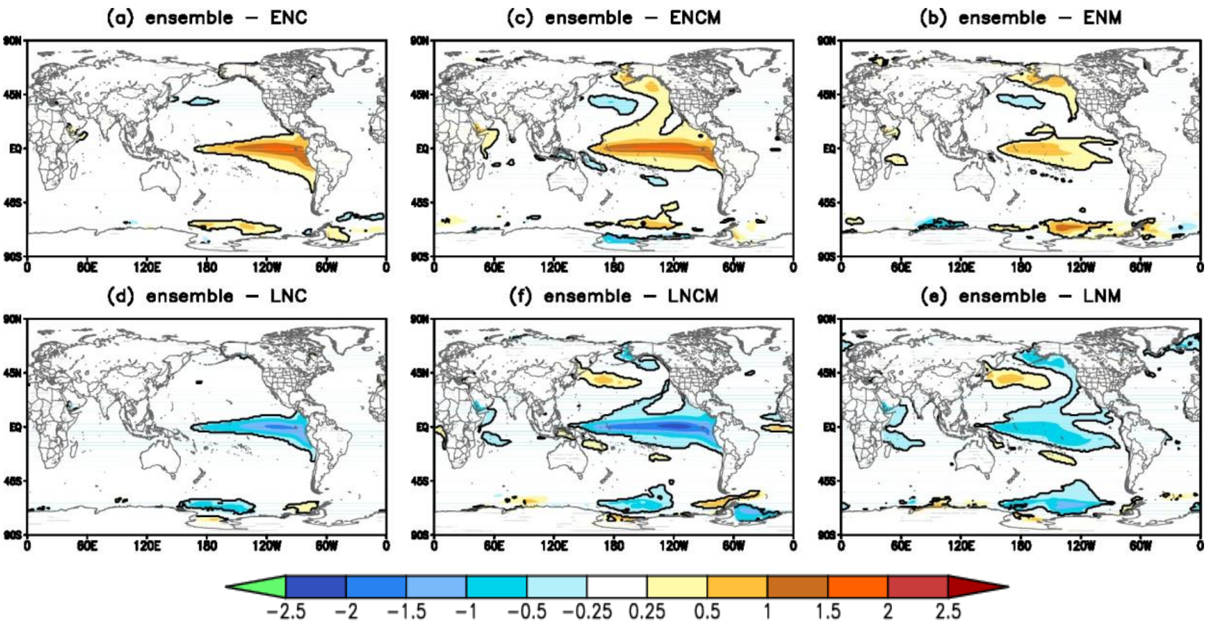

Fig. 14. Model ensemble mean of nine selected models for ISM (mm/day) and SST (°C) composites presented during JJA in different El Niño and La Niña cases. Ensemble mean ISM for El Niño are shown in the 1st row; (top left ENC, middle ENCM and right ENM). Ensemble mean of ISM for La Niña (2nd row), ensemble of SST for EN (3rd row) and ensemble of SST for La Niña (last row) are shown for respective cases.

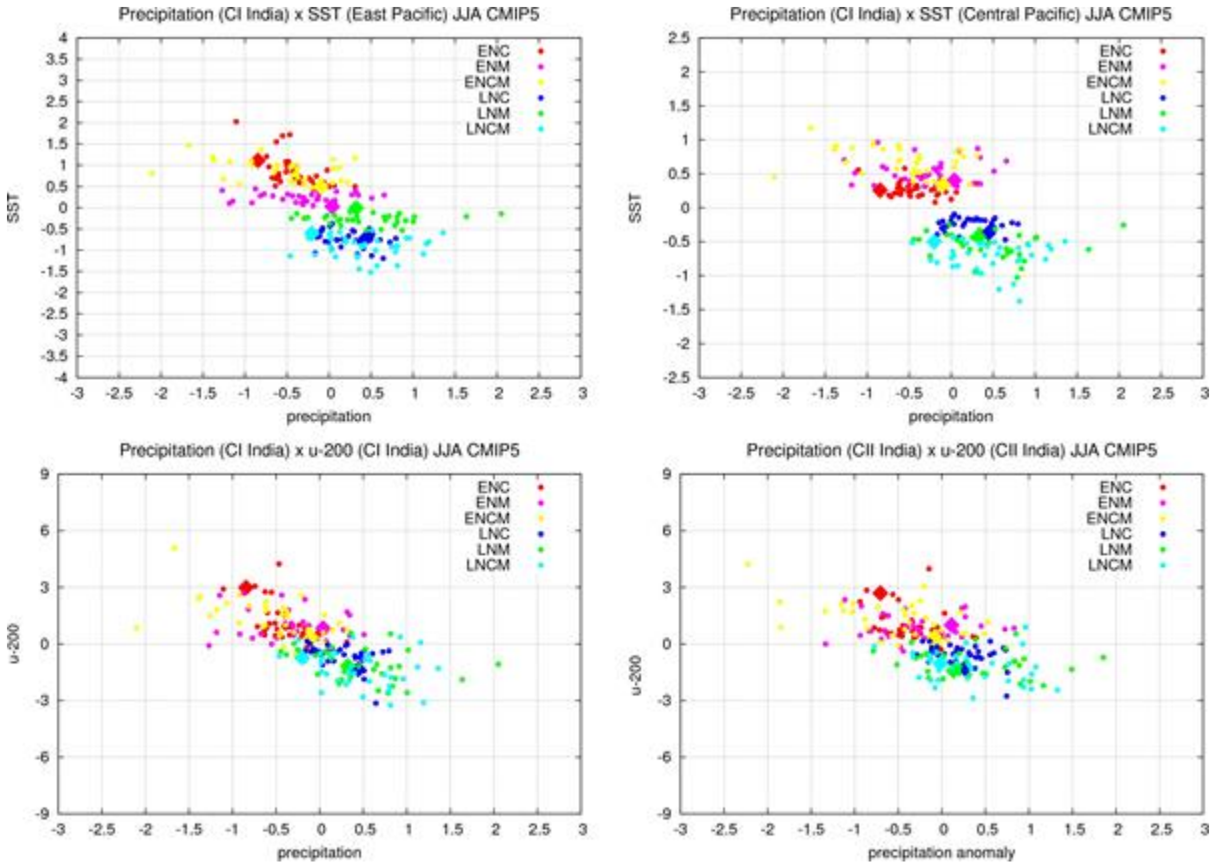

Fig 15. ISM precipitation (mm/day) around central India verses SST in tropical Pacific (top panel) and u-200 (m/s) (bottom panel) during JJA in different phases of El Niño and La Niña composites. Top panel considers SST around Central Pacific (left) and East Pacific (right). Bottom panel considers CI region (left) and CII region (right). Composites of ENC, ENM and ENCM are shown by red, pink and yellow respectively, whereas that of LNC, LNM and LNCM are shown by blue, green and cyan.

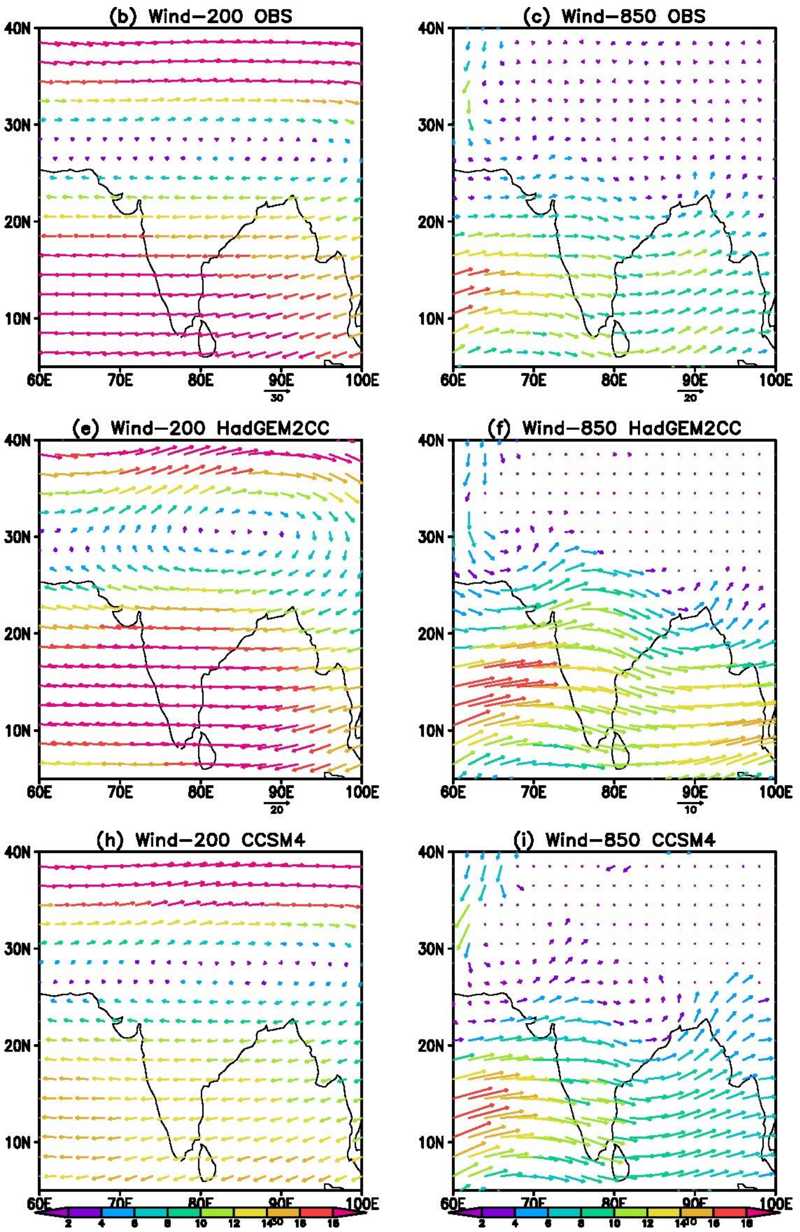

Supplementary Fig.1: The climatology of local wind fields at 200mb (left) and 850mb level (right) in m/s during JJA for period 1979 to 2005 in vector format. The top row for observed data, middle row for model HadGEM2-CC and the bottom row for model CCSM4.

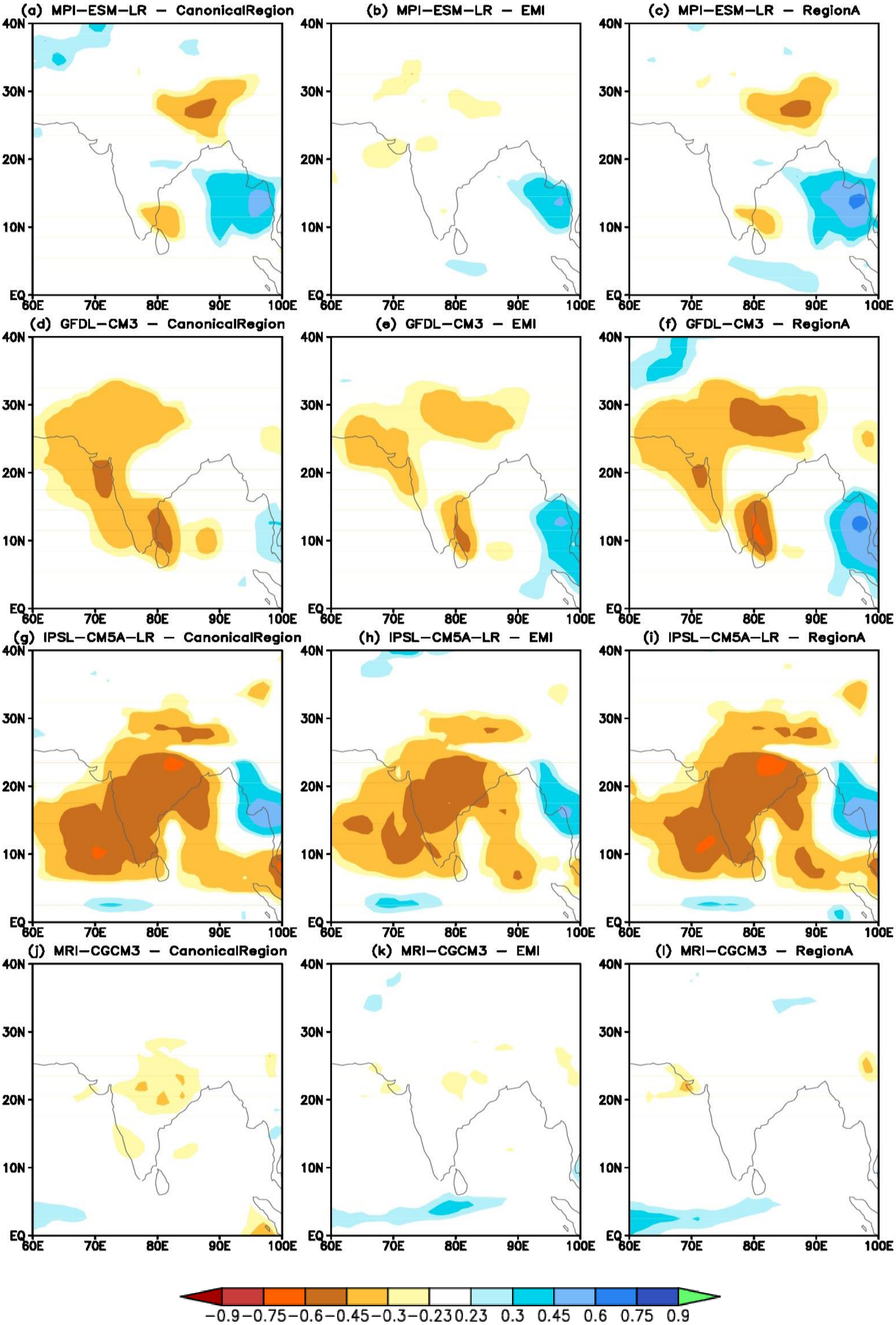
(a) MPI-ESM-LR – CanonicalRegion
(b) MPI-ESM-LR – EMI
(c) MPI-ESM-LR – RegionA
(d) GFDL-CM3 – CanonicalRegion
(e) GFDL-CM3 – EMI
(f) GFDL-CM3 – RegionA
(g) IPSL-CM5A-LR – CanonicalRegion
(h) IPSL-CM5A-LR – EMI
(i) IPSL-CM5A-LR – RegionA
(j) MRI-CGCM3 – CanonicalRegion
(k) MRI-CGCM3 – EMI
(l) MRI-CGCM3 – RegionA
40N
30N
20N
10N
EQ
60E
70E
80E
90E
100E
−0.9 −0.75 −0.6 −0.45 −0.3 −0.23 0.23 0.3 0.45 0.6 0.75 0.9

Supplementary Fig.2. Correlation between ISM (mm/day) with Canonical Region, EMI and Region A (JJA), in few models. Models closest in agreement with observations are MPI-ESM-LR and GFDL-CM3 (Top two panels); model generally -ve biased is IPSL-CM5A-LR (third panel); whereas, model almost showing neutral nature is MRI-CGCM3 (bottom panel).

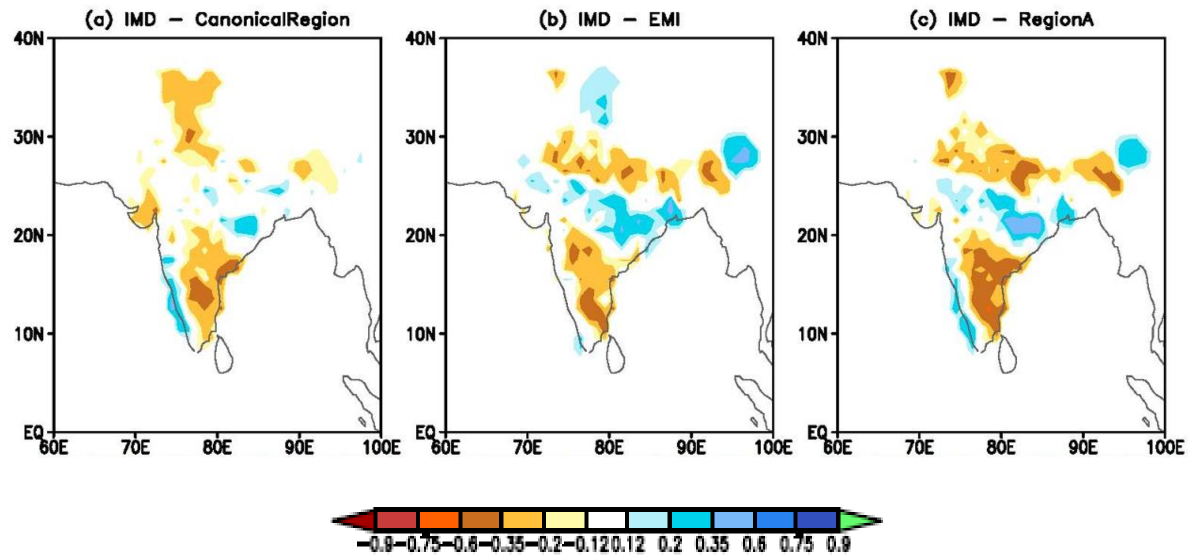

Supplementary Fig. 3: Correlation between ISM (mm/day) with Canonical Region (left), EMI (middle) and Region A (right) during JJA, using IMD gridded rainfall dataset. The colour scale ranges are slightly changed at lower values.

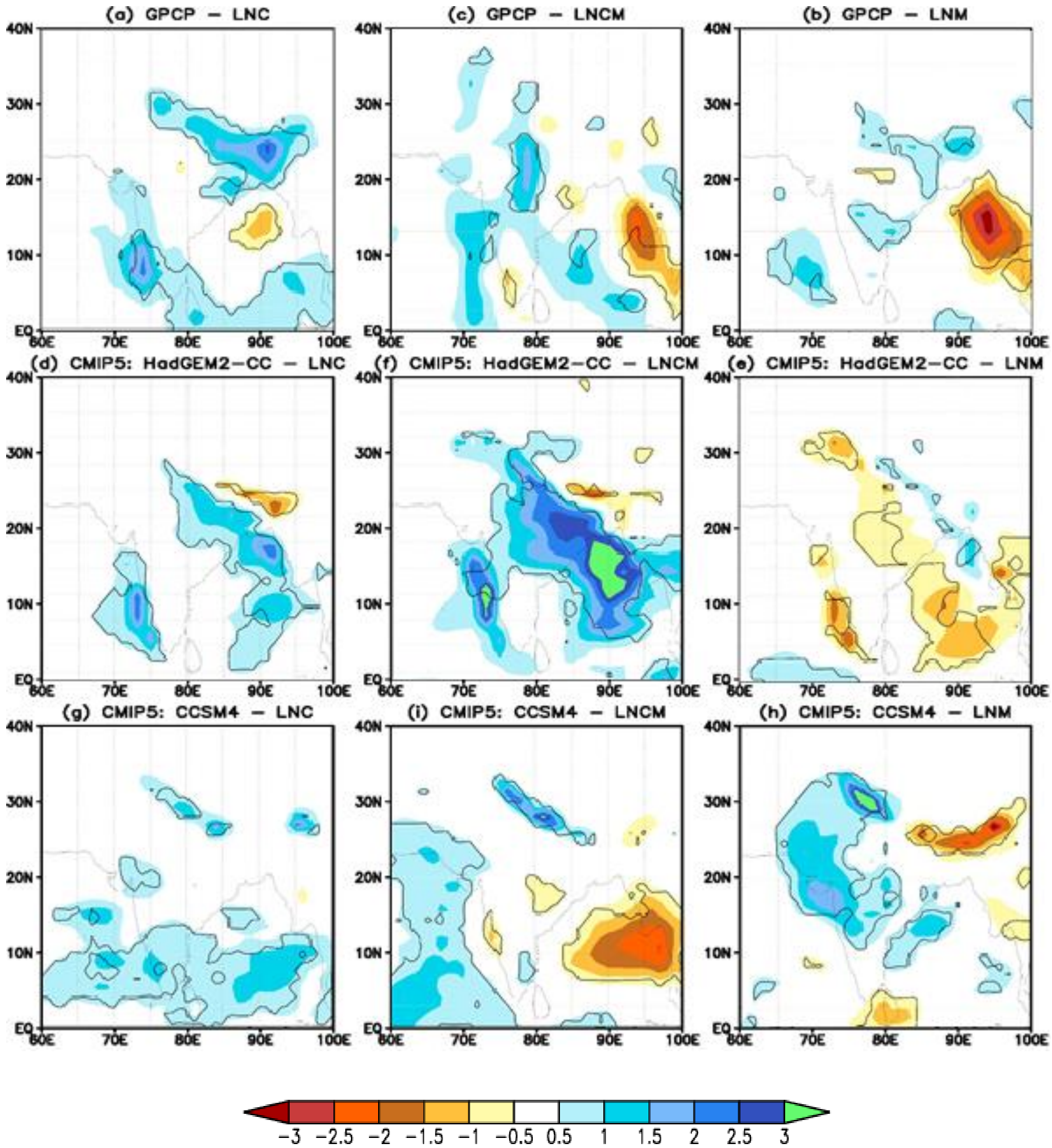

Supplementary Fig.4: Precipitation (JJAS) Composites (mm/day) for La Niña. Comparing one typical high top model (HadGEM2-CC) and one typical low top CMIP5 model (CCSM4) with observation (GPCP). Observations are shown in the top panel. Right panel is for composites in LNM years, left for LNC years and the middle for LNCM years.

Supplementary Table S1. ENSO years under each subcategory (ENC, LNC, ENM, LNM, ENCM, LNCM) as used for making composite analysis from observed SST and CMIP5 /AMIP5 simulations.

Observation (OBS) / CMIP5 Models	Year
Obs (HadISST)	
ENC	1983 1987 1997 2009
LNC	1984 1985 1988 2000 2007
ENM	1992 1994 2002 2004
LNM	1989 1998 2008
ENCM	1982 1991
LNCM	1999 2010
Obs (Hurrel for AMIP models)	
ENC	1983 1987 1997
LNC	1984 1985 1988 2000 2007
ENM	1992 1994 2002 2004
LNM	1989 1998 2008
ENCM	1982 1991
LNCM	1999
ACCESS1.0	
ENC	1863 1867 1869 1871 1874 1884 1887 1902 1908 1909 1916 1919 1922 1923 1925 1941 1942 1949 1954 1955 1968 1971 1975 1977 1978 1987 1988 1997 2004
LNC	1861 1865 1882 1885 1888 1890 1894 1895 1904 1906 1907 1911 1913 1920 1926 1931 1935 1936 1944 1953 1959 1963 1966 1967 1970 1976 1979 1981 1984 1985 1995 2002 2005
ENM	1864 1873 1930 1950 1989
LNM	1866 1880 1883 1891 1900 1910 1933 1964 1969 2003
ENCM	1868 1878 1914 1946 1999

LNCM	1889 1924
ACCESS1.3	
ENC	1868 1872 1873 1875 1879 1884 1887 1891 1894 1904 1913 1916 1919 1920 1923 1925 1928 1933 1946 1951 1963 1965 1969 1982 1998 2001 2004
LNC	1862 1874 1877 1885 1889 1892 1897 1903 1915 1917 1926 1938 1941 1944 1945 1949 1953 1964 1967 1971 1973 1975 1980 1984
ENM	1905 1910 1914 1922 1940 1947 1948 1970 1983 1991
LNM	1878 1883 1893 1927 1932 1950 1954 1961 1981 1989
ENCM	1869 1876 1900 1921 1936 1943 1958 1962 1972
LNCM	1867 1871 1882 1886 1890 1906 1918 1931 1960 1974 1976 1994
BCC-CSM1.1	
ENC	1866 1873 1882 1884 1885 1887 1889 1894 1895 1898 1902 1905 1926 1928 1934 1941 1942 1945 1950 1958 1973 1989 1991 1994 1996 2001
LNC	1863 1877 1880 1896 1899 1906 1908 1929 1935 1940 1947 1949 1953 1963 1965 1966 1972 1975 1977 1982 1985 1986 1990 1995 2002
ENM	1862 1879 1915 1931 1936 1988
LNM	1893 1917 1943 1968 1974 1987
ENCM	1864 1870 1871 1897 1919 1938 1948 1952 1962 1981 1999
LNCM	1865 1872 1886 1888 1916 1923 1946 1951 1956 1970 1980 2000
BCC-CSM1.1(m)	
ENC	1862 1866 1876 1883 1886 1889 1892 1894 1899 1903 1906 1909 1910 1918 1920 1932 1935 1939 1944 1955 1962 1966 1972 1976 1980 1998 2004
LNC	1863 1867 1877 1879 1885 1887 1895 1904 1908 1911 1913 1925 1936 1943 1945 1953 1960 1963 1965 1967 1969 1971 1973 1979 1984 1985 1987 1993 2003
ENM	1870 1871 1873 1884 1890 1900 1916 1923 1928 1948 1952 1956 2001 2005
LNM	1861 1872 1896 1905 1914 1921 1968 1977 2000
ENCM	1868 1912 1942 1951 1983 1989 2002
LNCM	1875 1882 1893 1898 1902 1919 1926 1933 1950 1982 1997 1999
BNU-ESM	
ENC	1875 1876 1879 1889 1899 1904 1929 1936 1947 1948 1954 1955 1968 1987 1992 2000 2005

LNC	1865 1878 1880 1886 1897 1916 1920 1921 1927 1930 1937 1940 1945 1953 1978
ENM	1867 1915 1971 1995 1997 2003
LNM	1861 1869 1898 1946 1976
ENCM	1863 1864 1870 1874 1881 1887 1896 1923 1935 1938 1957 1964 1974 1980 1986 1996 1999
LNCM	1890 1895 1905 1906 1909 1911 1934 1949 1956 1958 1965 1973 1984 1988 1993 2001 2004
CanESM2	
ENC	1867 1870 1873 1876 1881 1892 1894 1895 1903 1906 1911 1915 1916 1918 1922 1935 1937 1940 1944 1947 1951 1955 1965 1973 1982 1985 1990 1992 1995 2000
LNC	1865 1868 1875 1882 1885 1893 1904 1909 1913 1919 1923 1926 1930 1932 1934 1938 1949 1952 1954 1956 1966 1968 1971 1974 1976 1983 1986 1997 1999
ENM	1862 1874 1896 1900 1989 1996
LNM	1866 1905 1920 1924 1933 1950 1957 1958 1960 1975 1987 1998
ENCM	1879 1912 1948 1961 1977 1981 2005
LNCM	1902 1946 1978
CCSM4	
ENC	1879 1884 1885 1890 1894 1897 1901 1908 1926 1927 1933 1947 1976 1980 1992 1993 1997 2000 2001
LNC	1865 1873 1881 1906 1907 1910 1920 1937 1941 1944 1949 1962 1973 1977 1978 1984
ENM	1869 1875 1876 1891 1953 1965 1975 1983 1990 1991 2005
LNM	1866 1878 1887 1893 1899 1911 1925 1967 1996 1999
ENCM	1863 1864 1868 1872 1880 1909 1923 1930 1956 1969 1982 1986
LNCM	1877 1886 1892 1895 1903 1918 1921 1928 1932 1934 1948 1966 1971 1988 1994 1995 2003
CMCC-CM	
ENC	1867 1875 1876 1880 1884 1885 1889 1897 1900 1905 1906 1909 1915 1921 1926 1929 1930 1933 1934 1936 1937 1944 1949 1952 1953 1955 1956 1969 1978 1987 1993 2002 2004
LNC	1864 1877 1878 1883 1901 1907 1908 1910 1914 1918 1923 1931 1935 1939 1942 1943 1954 1960 1965 1971 1975 1985 1991 1996 1998 2005
ENM	1868 1888 1898 1903 1904 1925 1970 1984 1994 2000 2003

LNM	1862 1916
ENCM	1861 1891 1899 1982
LNCM	1865 1869 1893 1917 1922 1927 1945 1966 1974
CNRM-CM5	
ENC	1864 1865 1871 1879 1888 1896 1910 1919 1927 1941 1944 1946 1950 1956 1973 1990 1993 1997 1999 2004 2005
LNC	1866 1867 1870 1874 1894 1897 1905 1906 1912 1918 1932 1934 1938 1954 1958 1964 1966 1967 1969 1972 1988 1991 1998
ENM	1880 1914 1925 1928 1953 1962 1968 1976 1979 1989
LNM	1882 1904 1908 1920 1942 1947 1951 1963
ENCM	1877 1881 1892 1902 1903 1907 1911 1921 1924 1933 1935
LNCM	1872 1885 1889 1915 1945 1960 1974 1977 1980
CSIRO-Mk3.6.0	
ENC	1862 1865 1875 1878 1881 1886 1890 1896 1921 1942 1946 1949 1952 1957 1967 1982 1986 1995 1997 1998 1999 2004
LNC	1861 1889 1894 1895 1897 1905 1907 1913 1917 1920 1925 1932 1973 1974 1977 1993 1994 1996 2001
ENM	1864 1892 1893 1923 1928 1931 1943 1958 1959 1983 1984 1991 2005
LNM	1874 1884 1898 1902 1908 1914 1940 1951 1971 1978
ENCM	1887 1891 1903 1904 1911 1915 1918 1922 1936 1937 1941 1945 1964 1975 1976
LNCM	1867 1869 1901 1910 1919 1938 1948 1961 1966 1970 1981 1985
FGOALS-g2	
ENC	1862 1869 1872 1876 1877 1879 1890 1893 1898 1903 1912 1920 1923 1928 1936 1937 1940 1948 1953 1976 1984 1989 1990 1997
LNC	1863 1867 1870 1878 1884 1888 1894 1900 1913 1919 1926 1929 1938 1942 1946 1949 1952 1957 1958 1963 1967 1974 1985 1988 1994 1998
ENM	1866 1882 1887 1908 1980 1991 2003
LNM	1911 1945 1966
ENCM	1873 1880 1883 1896 1983 1996 2000 2002
LNCM	1874 1891 1905 1910 1921 1922 1925 1934
FGOALS-s2	

ENC	1864 1865 1875 1884 1885 1887 1890 1897 1899 1900 1901 1912 1916 1917 1922 1925 1927 1931 1951 1952 1956 1958 1972 1973 1987 1989 1991 1998 2000
LNC	1866 1873 1876 1891 1902 1909 1921 1923 1926 1929 1935 1941 1944 1949 1957 1962 1964 1966 1974 1976 1992
ENM	1863 1896 1907 1914 1934 1953 1982 1983 1996 2003 2005
LNM	1895 1903 1936 1942 1961 1963 1967 1979
ENCM	1870 1871 1955 1981 1988 2002
LNCM	1874 1894 1919 1930 1933 1938 1939 1946 1960 1977 1978 1999
INM-CM4	
ENC	1861 1864 1867 1869 1871 1876 1880 1893 1902 1908 1912 1928 1935 1942 1945 1951 1969 1972 1978 1981 1985 1991 1999 2001 2004
LNC	1862 1866 1872 1882 1887 1892 1906 1910 1914 1923 1926 1939 1940 1947 1950 1955 1956 1958 1959 1963 1975 1980 1986 2005
ENM	1881 1884 1885 1913 1979 1983 1984 1996
LNM	1889 1896 1901 1915 1918 1919 1946 1953 1977
ENCM	1898 1905 1925 1938 1948 1965 1982 1995
LNCM	1888 1899 1900 1909 1921 1933 1937 1967 1987 1997 1998
MIROC5	
ENC	1890 1899 1932 1951 1960 1965 1966 1975 1976 1993
LNC	1885 1901 1913 1941 1945 1957 1973 1977 1988 1998 2001
ENM	1873 1878 1884 1900 1908 1947 1961 2005
LNM	1865 1866 1875 1881 1886 1893 1914 1963 1969 1989
ENCM	1862 1868 1872 1877 1883 1889 1907 1911 1912 1921 1922 1930 1931 1943 1952 1959 1986 1992 2003 2004
LNCM	1864 1874 1879 1880 1891 1892 1924 1927 1933 1934 1953 1962 1967 1968 1978 1994 1995
NorESM1-M	
ENC	1861 1864 1871 1876 1883 1888 1891 1894 1900 1903 1910 1913 1916 1919 1924 1934 1942 1943 1946 1948 1951 1954 1960 1970 1983 1987 1996 1999 2003
LNC	1862 1867 1877 1878 1881 1885 1886 1904 1912 1915 1917 1920 1945 1949 1959 1961 1972 1974 1978 1984 1986 1994 1997
ENM	1865 1872 1880 1890 1899 1935 1938 1939 1955 1977 2004
LNM	1870 1887 1897 1902 1923 1936 1953 1964 1992 1995

ENCM	1868 1895 1956 1989
LNCM	1892 1893 1896 1901 1905 1930 1952 1963 1971 1991
GFDL-CM3	
ENC	1871 1873 1878 1882 1890 1905 1907 1910 1914 1917 1920 1922 1924 1926 1930 1934 1937 1941 1944 1948 1964 1972 1979 1982 1986 1998
LNC	1862 1876 1889 1891 1893 1902 1909 1916 1921 1923 1927 1929 1932 1933 1943 1949 1963 1969 1971 1978 1985 1987 1989 1991 1993 1994 1995 1999 2003
ENM	1861 1865 1868 1874 1899 1945 1960 1992 2002 2005
LNM	1863 1866 1877 1881 1885 1897 1911 1919 1939 1958 1981
ENCM	1864 1875 1883 1895 1898 1928 1951 1956 1962 1974 1984 1988 1996
LNCM	1896 1901 1906 1947 1966 1973 1976 1980
HadGEM2-CC	
ENC	1867 1870 1873 1878 1879 1881 1884 1900 1901 1904 1905 1920 1921 1927 1939 1945 1949 1951 1953 1958 1963 1975 1981 1986 1989 1990 1992 1993 1998 1999 2002 2004
LNC	1874 1877 1883 1886 1898 1903 1908 1910 1912 1916 1930 1931 1932 1937 1938 1942 1955 1956 1960 1961 1964 1965 1968 1971 1976 1983 1984 1987 1991 1995 1996
ENM	1864 1872 1906 1926 1928 1979
LNM	1891 1913 1936 1948 1966 1982
ENCM	1893 1919 1935 1962 1970 2003
LNCM	1890 1929 1940 1946 1947
GISS-E2-R	
ENC	1866 1877 1887 1891 1898 1901 1910 1914 1916 1918 1924 1928 1932 1934 1937 1948 1949 1962 1977 1979 1981 1985 1989 1990 1992 2000
LNC	1885 1888 1889 1892 1896 1902 1907 1915 1929 1936 1939 1946 1957 1961 1963 1964 1971 1972 1978 1986 1991 1997
ENM	1872 1873 1874 1943 1944 1952 1974 2004
LNM	1879 1908 1947
ENCM	1861 1862 1869 1883 1920 1973 1998
LNCM	1867 1884 1899 1921 1922 1926 1950 1955 1966 1984 1993 1996
IPSL-CM5A-LR	

ENC	1862 1865 1869 1874 1880 1885 1904 1926 1936 1938 1940 1948 1953 1959 1967 1975 1988 1992 1997 1999 2002 2005
LNC	1867 1872 1879 1882 1892 1894 1897 1900 1906 1909 1919 1930 1944 1964 1978 1979 1991 1994 1998
ENM	1870 1875 1911 1914 1918 1922 1923 1931 1954 2001
LNM	1887 1901 1917 1920 1935 1973 1986
ENCM	1881 1891 1907 1929 1943 1949 1960 1982 1989 1993 2000
LNCM	1866 1884 1889 1898 1933 1934 1937 1939 1942 1947 1957 1958 1968 1980 1985 1996
IPSL-CM5A-MR	
ENC	1864 1870 1872 1876 1886 1890 1905 1907 1919 1937 1939 1948 1954 1976 1979 1986 1989 1992 1998 2001
LNC	1863 1866 1871 1891 1897 1908 1917 1921 1926 1947 1955 1961 1967 1968 1974 1981 1988 1997 2000
ENM	1884 1896 1940 1950 1959
LNM	1875 1889 1909 1927 1932 1945 1963 1973 1985
ENCM	1861 1865 1873 1916 1920 1929 1935 1941 1949 1958 1964 1971 1980 1983 1987 1995 1996 2005
LNCM	1869 1874 1885 1887 1904 1923 1930 1931 1951 1952 1962 1975 1978 1984 1991
MPI-ESM-LR	
ENC	1866 1871 1872 1873 1878 1879 1884 1887 1888 1897 1903 1909 1912 1916 1919 1952 1955 1961 1962 1968 1972 1976 1979 1986 1989 1997 1998 2001
LNC	1865 1869 1885 1886 1900 1904 1910 1917 1923 1926 1937 1945 1950 1956 1959 1965 1969 1974 1977 1978 1981 1985 1995 2000 2004
ENM	1874 1876 1942 1973 1987 1999 2002
LNM	1870 1883 1891 1899 1911 1918 1938 1960 1970 1994 1996
ENCM	1867 1875 1913 1925 1934 1935 1941 1963 1980 1990 2003
LNCM	1882 1901 1907 1921 1927 1929 1943 1966 1992 1993
MPI-ESM-MR	
ENC	1862 1865 1870 1873 1902 1906 1913 1914 1919 1921 1924 1926 1929 1932 1938 1947 1952 1984 1993 1999 2001
LNC	1871 1888 1897 1898 1910 1915 1916 1917 1918 1922 1936 1942 1950 1959 1968 1969 1976 1979 1981 1987 1988 1994 1998
ENM	1879 1904 1905 1920 1927 1934 1946 1953 1954 1962 1970

LNM	1863 1899 1911 1937 1983 1995
ENCM	1866 1874 1883 1892 1896 1903 1945 1974 1975 1990 1996 1997 2000
LNCM	1868 1872 1877 1907 1908 1931 1943 1963 1964 1965 1977 1982
MRI-CGCM3	
ENC	1861 1864 1866 1878 1884 1885 1892 1895 1916 1919 1920 1927 1930 1934 1945 1948 1954 1960 1963 1998 2002
LNC	1869 1876 1883 1890 1896 1897 1899 1905 1906 1909 1911 1913 1917 1923 1925 1928 1943 1961 1962 1965 1972 1978 1983 1985
ENM	1871 1875 1889 1893 1939 1968 2001 2003
LNM	1887 1891 1926 1951 1966 1974 1987
ENCM	1862 1888 1898 1908 1941 1975 1977 1984 1988 1991 2004 1877 1886 1894 1929 1933 1944 1947 1950 1957 1959 1973 1980
LNCM	1986